Biomaterials Translational

Nanoformulation-assisted early diagnosis of prostate cancer: Advances and perspectives

Zhiyuan Zhou[1,2,3#], Mingyu Chang[1,2#], Jingcheng Lyu[1,2#], Jianhua Zhao[3], Zongwei Wang[4], Fengbo Zhang[5*], Yinong Niu[1,2*], and Boyu Yang[1,2*]

ABSTRACT

Prostate cancer is one of the most common cancers affecting men worldwide. Owing to late diagnosis, the mortality rate associated with prostate cancer remains relatively high. Traditional diagnostic methods are, in most cases, unfriendly to patients or have diagnostic lag defects. Further diagnosis requires prostate biopsy. The most common biomarker is prostate-specific antigen, which is quantified as the content of the prostate health index to describe the risk of prostate cancer. Traditional biochemical analysis methods are costly, time-consuming, and lack specificity. They are also limited by the detection range, preventing high sensitivity. The exploration of novel biomarkers has identified several promising alternatives. The development of integrated nanomaterial technology provides a feasible potential method for the rapid, sensitive and non-invasive determination of these biological markers and assists in the optimisation of imaging diagnosis, which is expected to solve the current challenges in the diagnosis of prostate cancer. This paper reviews the advances in the diagnostic screening and imaging of prostate cancer using nanostructure-based biofunctional sensors, probes and contrast agents such as gold nanoparticles, upconversion nanoparticles, quantum dots, and magnetic nanoparticles. It also highlights the potential of emerging paradigms in nanoarchitectonics to definitive cancer diagnosis.

Keywords:
Diagnosis; Nanoparticles; Prostate cancer; Prostate-specific antigen

#Authors contributed equally.

***Corresponding authors:**
Boyu Yang,
ybyurology@163.com;
Fengbo Zhang,
13701319061@139.com;
Yinong Niu,
18601020160@163.com

How to cite this article:
Zhou Z, Chang M, Lyu J, *et al.* Nanoformulation-assisted early diagnosis of prostate cancer: Advances and perspectives. *Biomater Transl.* 2025, 6(3), 232-249.
doi: 10.12336/bmt.24.00077

1. Introduction

Prostate cancer (PCa) is currently the most diagnosed cancer and the second leading cause of cancer death among men, with the exception of melanoma skin cancer, in North and South America, Europe, Australia, and the Caribbean. An estimated 268,500 men were diagnosed with PCa in 2022, and approximately 34,500 died from it.[1] The disease occurs mainly in elderly individuals with risk factors, including age, family history, and genetic predispositions, and the incidence rate gradually increases with age, reaching its highest level in those in their 70s.[2] PCa refers to an epithelial malignant tumour that occurs in the prostate. Adenocarcinoma accounts for more than 95% of the pathological types. PCa is a slow-progressing cancer that is easily overlooked in the early stages of the disease due to inconspicuous symptoms, and most people in China are consequently diagnosed in the middle and late stages. For early diagnosis of primary PCa with active surveillance and intervention, the rate of mortality at 15 years is 0.1%, and the risk of metastasis is less than 1%, whereas patients with aggressive biology or metastasis at initial presentation typically have a shorter overall survival.[3] Therefore, early diagnosis and identification of PCa is particularly essential in the clinical treatment and prognosis of patients.

The clinical diagnosis of PCa depends mainly on digital rectal examination, serum prostate-specific antigen (PSA), transrectal prostate ultrasound and pelvic magnetic resonance imaging (MRI).[4] Because of the high bone metastasis rate of PCa, radionuclide bone scanning is usually performed before the treatment plan is formulated. Pathological examination by prostate biopsy is the gold standard for the diagnosis of PCa.[5] The Gleason Grade Group (GGG) system is

commonly used to evaluate the degree of malignancy of PCa histologically and is divided into 2 to 10 points according to the sum of the scores of the main and secondary structural areas in cancer tissue.

PSA was approved by the U.S. Food and Drug Administration in 1984 as a marker for PCa because of its specificity for the prostate gland.[6] Its normal function is to liquefy semen, but it is significantly overproduced in PCa. A serum PSA concentration above 4.0 ng/mL is considered a positive indicator for PCa, but this standard is increasingly considered arbitrary. Other conditions, such as ageing, benign prostatic hyperplasia and prostatitis, can also lead to elevated PSA levels, so the possibility of false-positives is very high.[7] In addition, the PSA values of some PCa patients are less than 4 ng/mL, so the test is not always reliable and does not distinguish between PCa stages. Traditional diagnostic methods for PCa seem insufficient for early and accurate cancer diagnosis, prompting global efforts to develop new biomarkers and instruments for precise early detection.

Recently, nanotechnology, with key elements less than 100 nm in diameter, has emerged as a promising diagnostic strategy for tumour detection and screening. Owing to the low cost, high efficiency and targeting specificity of nanomaterials, nanotechnology-based detection methods provide opportunities and candidates for the early diagnosis of PCa.[8] This approach not only compensates for the limitations of traditional biochemical detection and the singleness of detection methods but also realises multimodal scene applications for screening or recurrence monitoring. In addition, the fabrication of nanostructured probes is well realised in imaging detection, which may become an ideal platform for high-precision imaging improvement.[9] Given the superior binding capacity of functionalised nanoparticles to PCa biomarkers, we summarise the advancements in the nanotechnology-assisted detection of PCa. In this review, we first emphasise the progress of nanotechnology-assisted PSA detection and then illustrate the development status of nanomaterials or nanosensors combined with other non-PSA PCa biomarkers, as well as their breakthroughs in imaging technology optimisation (**Figure 1**). Finally, we anticipate the ever-evolving future and explore the possibility of using nanotechnology in the early diagnosis of PCa.

This review investigates the integration of biological nanomaterials and clinical medicine, offering an in-depth comprehension of current nano-engineering research focused on the early diagnosis of PCa. A systematic literature search was conducted in PubMed using the keywords "nanomaterial", "diagnosis", "prostate cancer", and "prostate-specific antigen". The search was limited to studies published in English language peer-reviewed journals. The primary selection criteria emphasised the relevance of nanomaterial-based probes, sensors, and imaging contrast agents specifically for PCa diagnosis and screening. Only articles directly pertinent to this study's focus were included, excluding commentaries and unrelated research.

2. Auxiliary enhancement of prostate-specific antigen detection

Currently, biochemical detection of PSA is still the most commonly used tool for PCa screening.[10] The widespread implementation of PSA testing has contributed to the increased detection rate of PCa in China. Higher PSA levels are directly associated with cancer risk and PCa stage. However, some patients with new-onset PCa still have serum PSA levels below 4 ng/mL, and those with low PSA levels also have a 15% chance of developing PCa.[11,12] Therefore, the free/total PSA ratio stratifies risk within the clinically ambiguous range (PSA 4-10 ng/mL) as per European Association of Urology (EAU) guidelines. For more accurate detection of PSA and subsequent diagnosis, strategies for applying various nanotechnologies to help optimise PSA testing procedures have played an indispensable role in PCa health care decisions (**Table 1**).

2.1. Gold nanoparticles

The most distinctive feature of noble metal nanoparticles, such as gold nanoparticles (AuNPs), is their localised surface plasmon resonance (LSPR) property. Specifically, when incident light irradiates AuNPs and the frequency of incident photons coincides with the vibration frequency of AuNPs, it will exert a vigorous absorption effect on the photon energy. This LSPR absorption phenomenon is one of the principal bases for the application of AuNPs in the detection field.

Funari *et al.*[13] introduced a compact opto-microfluidic sensor featuring a substrate of gold nanospikes with enhanced sensitivity. This nanomaterial enables the precise and concurrent measurement of PSA, with a limit of detection (LOD) of 0.22 ng/mL. Yeh *et al.*[14] presented a biopolymer-preserved plasmonic biosensor with improved stability for the sensitive detection of PSA, which was characterised as a yolk–shell plasmonic nanomaterial consisting of solid AuNPs as the core and a gold/silver nanocage as the shell. The biosensor was proven to achieve a limit of PSA detection of 10 pg/mL. Gao *et al.*[15] prepared a core-satellite nanoprobe, polydopamine (PDA)-Au, by using cysteine (Cys) as the linker to assemble PDA nanospheres and Au seeds. Specifically, Cys was employed to modify gold seeds by facilitating the formation of Au–S bonds, which occur through the interaction of the –SH group in Cys with the Au atoms on the surface of the Au seeds. The –NH2 group in Cys subsequently forms a bond with PDA via a Michael addition reaction, resulting in a stable core-satellite structure known as PDA-Au. On the basis of the observed remarkable dual-mode responses, a colourimetric and photothermal immunoassay was developed for detecting PSA. The LSPR

[1]Department of Urology, Beijing Friendship hospital, Capital Medical University, Beijing, China; [2]Institute of Urology, Beijing Municipal Health Commission, Beijing, China; [3]Department of Neurosurgery, Shanghai Pudong New Area Gongli Hospital, Shanghai, China; [4]Beth Israel Deaconess Medical Center, Department of Surgery, Harvard Medical School, Boston, MA, United States of America; [5]Beijing Luhe Hospital, Capital Medical University, Beijing, China

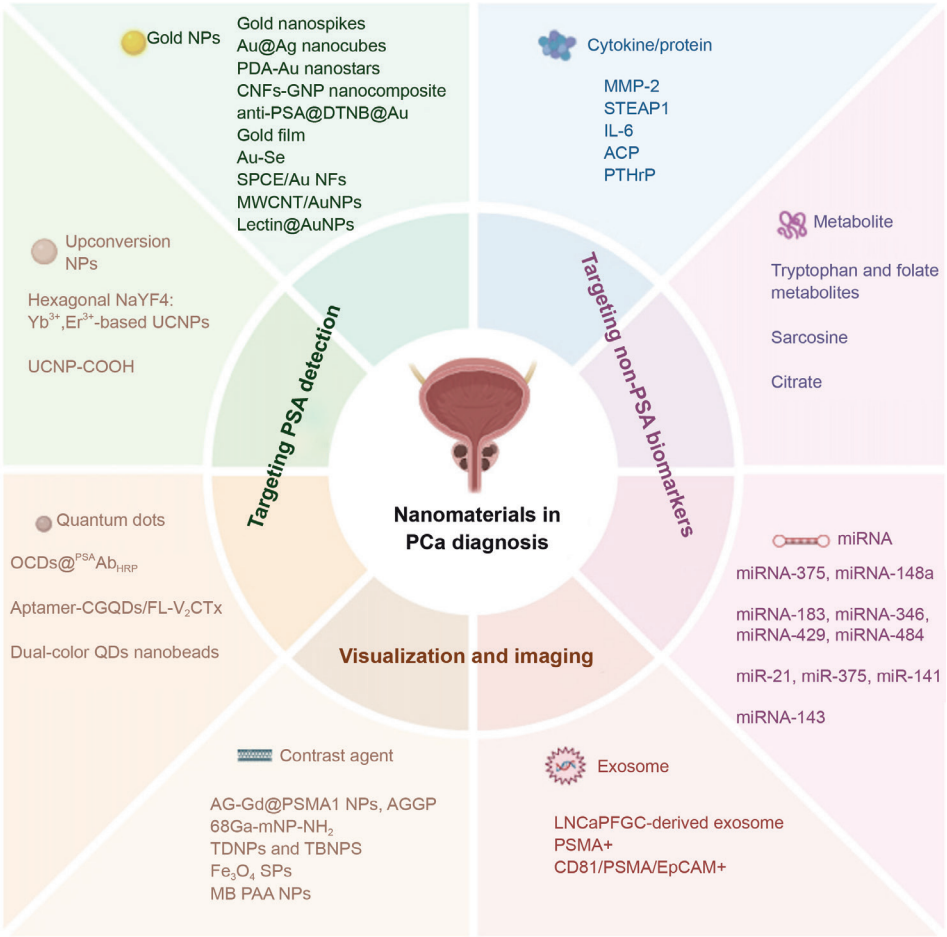

Figure 1. Schematic illustration of the application of emerging nanomaterials in the detection and diagnosis of PCa.
Abbreviations: ACP: Acid phosphatase; Ag: Argentum; AGGP: AG-Gd@PSMA1 NPs; SPCE: Screen-printed carbon electrodes; Au: Gold; CGQD: Carboxyl graphene quantum dot; EpCAM: Epithelial cell adhesion molecule; FGC: The fast colony line, a derivative of LNCaP cell line; GNP: Gold nanoporous; IL-6: Interleukin-6; MB PAA: Methylene blue polyacrylamide; MMP-2: Matrix metalloproteinase 2; mNP: Magnetic iron oxide nanoparticle; MWCNT: Multi-walled carbon nanotubes; NF: Nanoflower; NP: Nanoparticle; OCDs: S-doped carbon dots; PCa: Prostate cancer; PDA: Polydopamine ; CNF: Carbon nanofibers; PSA: Prostate-specific antigen; PSMA: Prostate specific membrane antigen; PTHrP: Parathyroid hormone-related protein; QD: Quantum dot; SP: Supraparticles; STEAP1: Six-transmembrane epithelial antigen of the prostate 1; TBNP: Targeted bovine serum albumin with PSMA-11-HBED peptide; TDNP: Targeted carboxymethylated dextran with PSMA-11-HYNIC peptide; UCNPs: Upconversion nanoparticles.

peak of PDA-Au redshifted from 520 to 580 nm as the PSA concentration increased, and the colour of the solution changed from pink to purple, as measured by immunoassay. Moreover, the LOD of PSA was reduced to 6.71 pg/mL, which is below the threshold of 4 ng/mL in clinical practice. This dual-mode immunoassay combined with colourimetric and photothermal methods could provide more reliable, convenient and accurate screening of potential PCa (**Figure 2**). Felici *et al.*[16] presented a portable and reusable microfluidic platform integrated with a carbon nanofibre-decorated gold nanoporous sensing device for serum PSA quantification with a detection limit of 5 pg/mL and a linear range of 0.01 to 50 ng/mL. Additionally, Turan *et al.*[17] introduced a novel analytical method with magnetic molecularly imprinted polymers as an antibody-free capture probe and labelled it with anti-PSA-modified AuNPs and an enhanced Raman reporter, ensuring both high selectivity and sensitivity for the determination of PCa.

To detect PSA in a small sample and in a short time, He *et al.*[18] prepared a nanosensing electrode by regulating the wrinkles of the sensor with a 200 nm thick gold film, which was validated by a label-free immunoassay in 20 μL of serum within 35 minutes. It exhibited not only a LOD of 0.38 fg/mL, the lowest among those of label-free PSA sensors, but also a high sensitivity to PSA, almost 3.9 times that of a planar electrode. Furthermore, to overcome the shortcomings of AuNPs resulting in false-positive results in biological systems, Au–Se-bonded nanoprobes were designed and constructed on the basis of the fluorescence resonance energy transfer (FRET) effect with extraordinary anti-interference ability and a detection range of 1–40 ng/mL.[19] Dou *et al.*[20] constructed a carbon interface modified with gold nanoflowers, which increased the number of PSA capture antibodies and further improved the signal-to-noise ratio of detection. In particular, Alnaimi *et al.*[21] proposed an electrochemical biosensor functionalised with multiwalled carbon nanotubes modified with AuNPs to detect PSA, which

Table 1. Recent advances in the development of NP-based nanosensors or nanoprobes assisting in PSA detection

NP	Final compound	Detection approach	LOD	Linear range	References
AuNPs	Gold nanospikes	Opto-microfluidic sensor	0.22 ng/mL	0–200 ng/mL	13
	Au@Ag nanocubes	Biopolymer-preserved plasmonic biosensor	10 pg/mL	10–100000 pg/mL	14
	PDA-Au nanostars	Colourimetric and photothermal immunosensor	6.71 pg/mL	0.05–100 ng/mL	15
	CNFs-GNP nanocomposite	Microfluidic electrochemical immunosensor	5 pg/mL	0.01–50 ng/mL	16
	Anti-PSA@DTNB@Au	Plasmonic sensor	0.9 pg/mL	0.5 pg/mL–1 μg/mL	17
	Gold film	Shrink polymer based electrochemical sensor	0.38 pg/mL	10 fg/mL–1000 ng/mL	18
	Au–Se	Au–Se bonded nanoprobe	–	1–40 ng/mL	19
	SPCE/Au NFs	EIC biosensor	0.28 ng/mL	0–100 ng/mL	20
	MWCNT/AuNPs	Label-free electrochemical biosensor	1 pg/mL	1–100 ng/mL	21
	Lectin@AuNPs	Biolayer interferometry sensor	0.04 μg/mL	0–0.4 μg/mL	23
UCNPs	Hexagonal NaYF4:Yb^{3+},Er^{3+}-based UCNPs	MTP based and MB-based ULISA	0.46 pg/mL	0.08–2.06 ng/mL	27
	UCNP-COOH	Fluorescence lateral flow test strip	0.1 ng/mL	0.1–100 ng/mL	28
QDs	OCDs@$^{PSA}Ab_{HRP}$	Electrochemical immunoassay	38 pg/mL for ECIA, 55 pg/mL for FIA	0.1–100 ng/mL, 5–120 ng/mL	31
	Aptamer-CGQDs/FL-V_2CTx	Fluorescence aptasensor	0.03 ng/mL	0.1–20 ng/mL	32
	Dual-colour QDs nanobeads	Flow cytometry	45 pg/mL for c-PSA, 22 pg/mL for f-PSA	0.2–50 ng/mL, 0.64–80 ng/mL	33

Abbreviations: Ag: Argentum; Au: Gold; AuNP: Gold nanoparticle; CGQDs/FL-V2CTx: Carboxyl graphene quantum dots/few-layer vanadium carbide; CNF: Carbon nanofibers; c-PSA: Complexed prostate-specific antigen; DTNB: 5,5′-dithiobis-(2-nitrobenzoic acid); ECIA: Electrochemical immunoassay; EIC: Electrochemical immunochromatography; FIA: Fluorescence immunoassay; f-PSA: Free prostate-specific antigen; GNP: Gold nanoporous; LOD: Limit of detection; MB: Magnetic microbead; MTP: Microtiter plate; MWCNT: Multi-walled carbon nanotubes; NF: Nanoflower; NP: Nanoparticle; OCDs@PSAAbHRP: The S-doped carbon dots bioconjugated with HRP-conjugated PSA antibody; PDA: Polydopamine; PSA: Prostate-specific antigen; QD: Quantum dot; Se: Selenium; SPCE: Screen-printed carbon electrodes; UCNP: Upconversion nanoparticles; ULISA: Upconversion-linked immunosorbent assays.

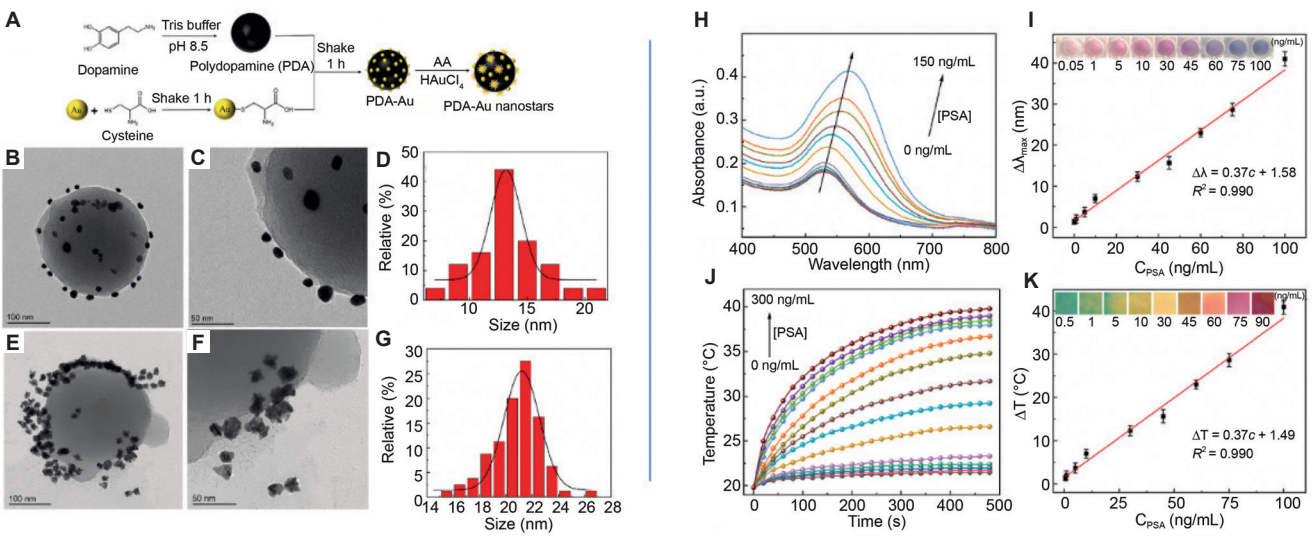

Figure 2. (A) Schematic illustration of the preparation of the core-satellite nanoprobe PDA-Au using cysteine as a linker. (B) TEM image of PDA-Au. Scale bar: 100 nm. (C) HRTEM image of PDA-Au. Scale bar: 50 nm. (D) Size distribution histograms for the Au seeds on PDA. (E) TEM image of PDA-Au after enzyme-mediated Au seed growth. Scale bar: 100 nm. (F) HRTEM image of PDA-Au after enzyme-mediated Au seed growth. Scale bar: 50 nm. (G) Size distribution histograms for the Au nanostars on PDA. (H) UV–Vis absorption spectra of the PDA-Au nanoprobe exposed to various concentrations of PSA. (I) Linear correlation of the redshift of the LSPR peak (Δλmax) with the PSA concentration (inset: corresponding photographs). (J) Temperature curves for PDA-Au upon the addition of different concentrations of PSA. (K) Linear relationship between the temperature increase (ΔT) and the PSA concentration (inset: corresponding photographs obtained via the infrared imager). Reprinted with Gao *et al.*[15] Copyright 2023, Elsevier B.V.

Abbreviations: AA: Ascorbic acid; Au: Gold; $HAuCl_4$: Chloroauric acid; HRTEM: High resolution transmission electron microscope; LSPR: Localised surface plasmon resonance; PDA: Polydopamine; PSA: Prostate-specific antigen; TEM: Transmission electron microscope; UV–Vis: Ultraviolet-visible light detector; ΔT: Temperature increase.

further shortened the detection time to approximately 5 minutes.

It is well known that glycoforms can indicate the pathogenesis state. Changes in the glycosylation patterns on the PSA protein backbone can indicate whether PCa is aggressive. Lectins have been reported to be superior biorecognition elements or detection probes for glycosylated cancer.[22] On this basis, lectin@AuNPs were manufactured for sensitive detection and

discrimination of PSA glycoforms with signal enhancement capacity.[23] This system could detect specific glycoforms of PSA down to 0.04 mg/mL and was easily automated with quantitative data output. This approach is complementary to certain low-cost methods, such as lateral flow immunoassay (LFIA) or conventional enzyme-linked immunosorbent assay (ELISA) analysis, and could also be applied in the identification of other glycoform-related diseases.

2.2. Upconversion nanoparticles

Upconversion nanoparticles (UCNPs) are nanomaterials that are capable of generating high-energy photons by means of an upconversion process subsequent to the absorption of lower-energy photons. This type of material possesses high light conversion efficiency, low excitation energy, and excellent photostability, thereby rendering it extensively applicable in fields such as optoelectronics, theranostics and, particularly, PCa detection.[24-26]

The sensitivity of conventional immunochemical analysis applied in the clinic is often not satisfactory for early diagnosis, so novel detection methods are needed. Makhneva *et al.*[27] reported that, compared with horseradish peroxidase and carboxyfluorescein, photon-UCNPs achieved the highest signal-to-background ratios (97.5) and the lowest LOD (0.46 pg/mL) for PSA. Hu *et al.*[28] developed a novel UCNP-based fluorescence lateral flow test strip for qualitatively and quantitatively detecting PSA. Specifically, UCNPs were synthesised using a conventional solvothermal method. The UCNPs subsequently underwent modification through a one-step process involving a carboxylated polymer to yield UCNP-COOH. Finally, they conjugated the corresponding anti-PSA antibodies to UCNP-COOH utilising a modified 1-ethyl-3-(3-dimethylaminopropyl) carbodiimide hydrochloride (EDC) and N-hydroxysuccinimide (NHS) coupling strategy to prepare the UCNP probe (**Figure 3**). The dose-dependent luminescence enhancement showed good linearity in the PSA concentration range from 0.1 to 100 ng/mL. In addition, the test strip showed excellent accuracy, anti-interference ability and stability, with consistency between the serum and fingertip blood samples, especially in the clinical grey zone. Therefore, UCNP point-of-care testing strips can achieve accurate detection of low-abundance PSA in serum and post-operative monitoring of PCa.

2.3. Quantum dots

Quantum dots (QDs) represent a type of semiconductor nanocrystal with distinctive electronic properties. The exceptionally high surface area/volume ratio bestows outstanding optical characteristics that are distinct from those of traditional luminescent materials. Owing to the diverse physical effects of QDs, such as the quantum size effect and surface effect, their advantages in terms of photostability, narrow emission spectra, low toxicity, and biocompatibility render them ideal candidates for applications in bioimaging, diagnosis, and biosensing.[29,30]

The bimodal assay via fluorescence immunoassay and electrochemical immunoassay helps to verify the feasibility of the clinical translation and application of QD nanomaterials. A nanoprobe was designed to detect PSA by biocoupling S-doped carbon dots with an antibody (OCDs@^{PSA}AbHRP), which widened the linear range of 0.1 to 100 ng/mL for electrochemical immunoassay and 5 to 120 ng/mL for fluorescence immunoassay.[31] The newly developed paper-based and smartphone-integrated fluorescence immunoassay relying on the OCDs@^{PSA}AbHRP probe provided effective and rapid detection, whereas the electrochemical immunoassay enabled high sensitivity and a low limit of 38 pg/mL for PSA detection (**Figure 4**). The carbon QD-based bimodal bioanalytical system is expected to be a promising alternative for traditional biochemical analysis. Zhu *et al.*[32] fabricated a

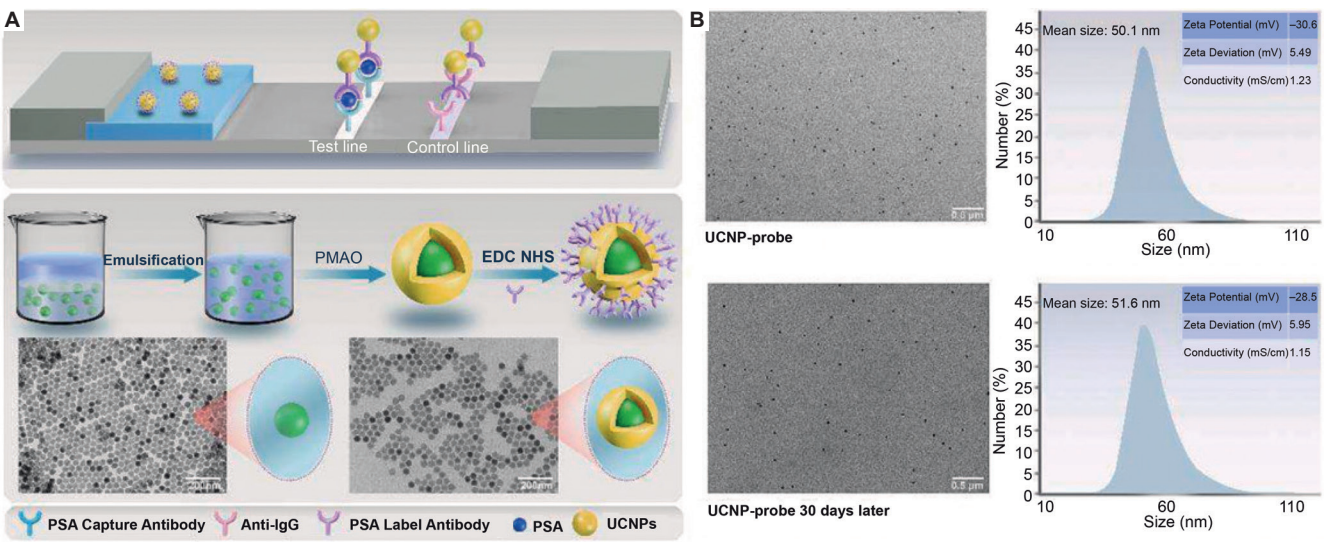

Figure 3. (A) Schematic diagram of the fluorescence lateral flow immunochromatographic assay strips (upper panel). Synthetic route of the UCNP-probe (lower panel). (B) TEM images of the hydrated particle size and zeta potential analysis results for the UCNP-probe and UCNP-probe after 30 days of storage. Scale bars: 0.5 μm. Reprinted with Hu *et al.*[28] Copyright 2023, Elsevier Inc.
Abbreviations: EDC: 1-ethyl-3-(3-dimethylaminopropyl) carbodiimide hydrochloride; NHS: N-hydroxysuccinimide; PMAO: Poly(methyl acrylate); PSA: Prostate-specific antigen; TEM: Transmission electron microscope; UCNP: Upconversion nanoparticles.

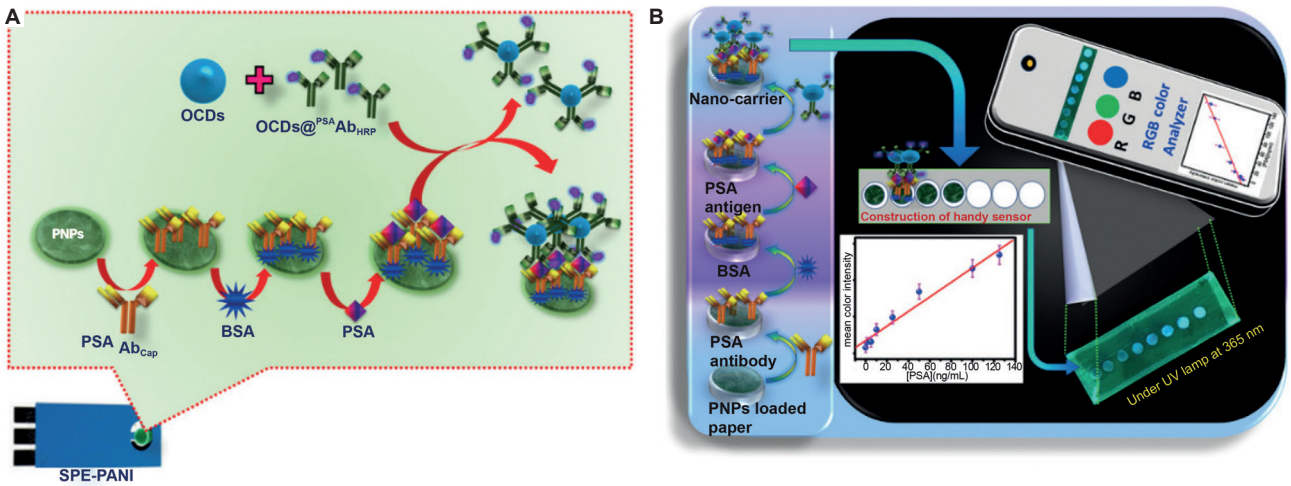

Figure 4. (A) Schematic representation of sandwich immunosensor fabrication for PSA detection depicting signal amplification by OCDs during an electrochemical immunoassay. (B) Schematic representation of smartphone paper-based optical sensors for the detection of PSA biomarkers. Reprinted with Korram *et al.*[31] Copyright 2023, Royal Society of Chemistry.
Abbreviations: BSA: Bovine serum albumin; OCDs: S-doped carbon dots; OCDs@$^{PSA}Ab_{HRP}$: The S-doped carbon dots bioconjugated with HRP-conjugated PSA antibody; PSA: Prostate-specific antigen; $^{PSA}Ab_{Cap}$: A capture antibody conjugated PSA; PNPs: Polyaniline nanoparticles; SPE-PANI: Polyaniline nanofiber-modified screen-printed electrode; UV: Ultraviolet.

novel graphene QD-based fluorescence aptasensor of PSA using a few-layer vanadium carbide (FL-V2CTx) nanosheet as a quencher, providing a linear detection range from 0.1 to 20 ng/mL with a limit of 0.03 ng/mL. Min *et al.*[33] developed a novel suspension microarray system based on dual-colour QD nanobeads as fluorescence labels for simultaneous detection of free prostate-specific antigen (fPSA) and complexed prostate-specific antigen (cPSA) with sensitivities of 45 and 22 pg/mL, respectively, showing excellent reliability in the grey zone.

Notably, the advancement of nanostructure-based PSA sensors, conversely, has an optimising impact on the supporting analytical approaches. This two-way, synergistic influence of integrating the analytical method and hardware structure further enhances the efficiency of detection. Alternatively, the existing analytical methods can be enhanced and supplemented with specific nanoprobes, and ultimately, a more stable and efficient detection instrument can be attained. The LFIA system has been used for cost-effective and rapid detection in recent decades and has become an ideal candidate for the point-of-care testing of PSA.[34] However, traditional LFIA methods have the drawbacks of low sensitivity and specificity. Gong *et al.*[35] designed an antibody-modified dendritic mesoporous silica@Prussian blue (DMSN@PB) nanozyme that served as an immunological probe in an enzymatic-enhanced colourimetric and photothermal dual-signal LFIA for PSA detection. DMSN was synthesised via the Stöber sol-gel method, subsequently reacted with the coupling agent triethoxysilane and modified with -NH2 groups to produce the intermediate DMSN-NH2. The surface -NH2 groups can capture Fe^{3+} ions. Concurrently, Fe^{3+} and $[Fe(CN)^{63-}$ were assembled in situ to form PB nanocrystals, ultimately yielding DMSN@PB nanocomposites. The colourimetric signal amplification and excellent photothermal conversion properties improve the anti-interference ability and sensitivity of LFIA, resulting in a wide linear range of 1–40 ng/mL and a low LOD of 0.202 ng/mL. The DMSN@PB-based LFIA provides a more accurate and reliable analysis for early PCa diagnosis. The combination of resonance Raman scattering and photoluminescence helps in the development of an accurate and sensitive dual-mode immunosensor strategy for PSA detection (**Figure 5**). Wang *et al.*[36] developed ZnS:Mn^{2+} nanoprobes on the basis of resonance Raman scattering and photoluminescence with an LOD of 113 ag/mL, indicating high sensitivity and potential for application in clinical practice.

3. Diagnostic biofunctionalised nanomaterials

To date, conventional methods such as ELISA have been widely used for PSA detection. However, these methods are time-consuming and usually involve specialised and expensive equipment or complicated sample pre-treatment. Most importantly, the high positive rate of the existing PSA test leads to excessive diagnosis and treatment of PCa to a certain extent, which indirectly increases the social and economic burden and the unfriendly experience of patients. In addition, traditional PSA detection cannot identify the stage and malignancy of PCa. Therefore, the development of reliable, rapid, and selective methods with non-PSA or multiple targets combined with PSA is highly important. As cancer research has progressed, certain non-PSA tumour markers have been identified as reliable tools for predicting the behaviour of PCa and helping clinicians specify the molecular mechanisms of tumourigenesis (**Table 2**). The sensitivity and specificity of these markers have gained broader attention with the use of various biofunctional nanomaterials for the early detection and staging of PCa.

3.1. Cytokines and proteins

Matrix metalloproteinase 2 (MMP-2) is a zinc-dependent secreted endopeptidase, and its overexpression is related to PCa tumourigenesis.[37,38] Detection of the MMP-2 protein level is beneficial for the early diagnosis of PCa. To

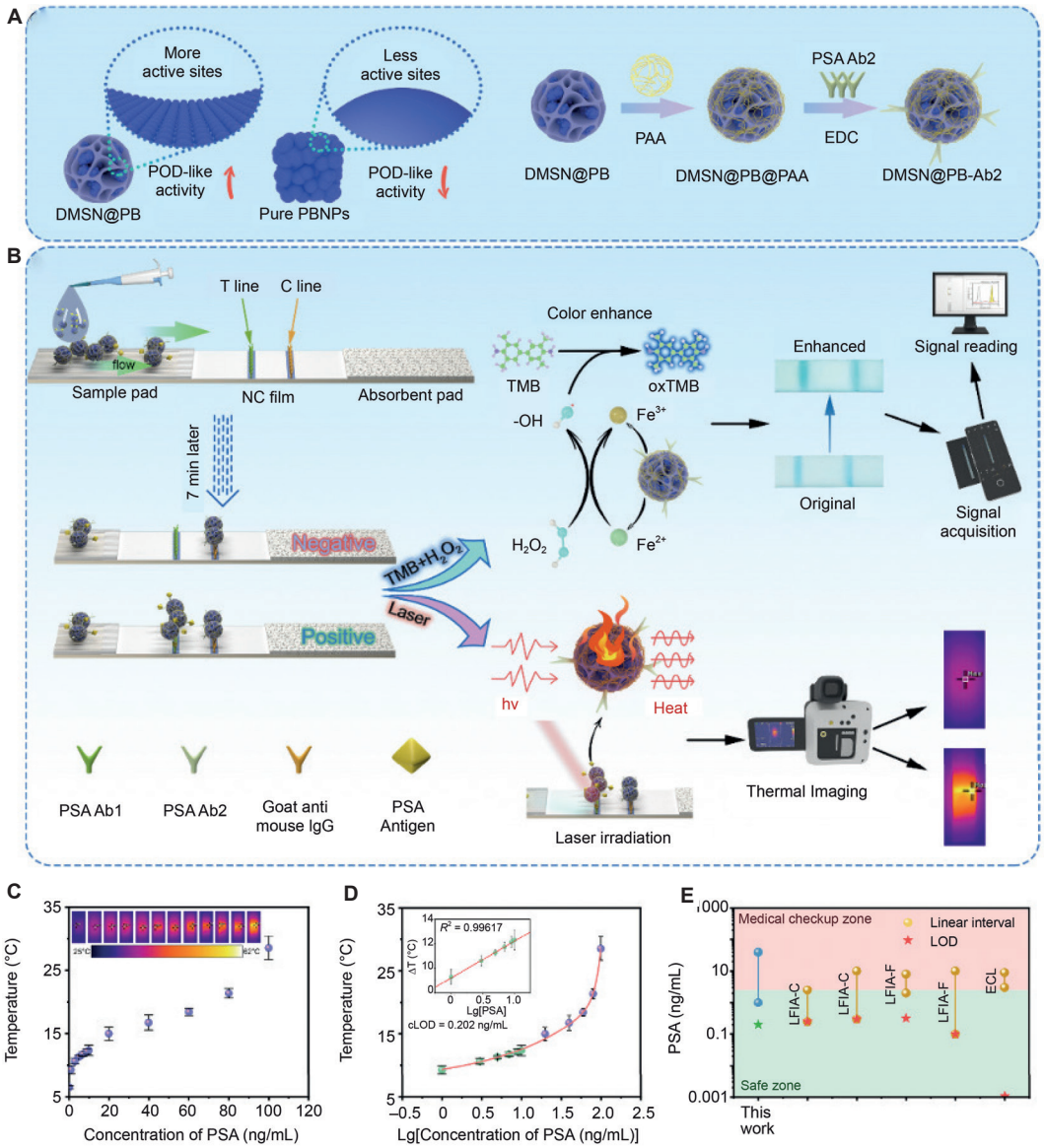

Figure 5. (A) Microstructure of DMSN@PB and pure PBNPs and antibody modification process of the DMSN@PB-Ab2 probe. (B) Principle of the DMSN@PB-based LFIA with dual signals for PSA detection. (C, D) Calibration curve and LFIA photos (C) and dynamic linear range using the photothermal signal (D). (E) Comparison of different methods for detecting PSA. Reprinted with Gong *et al.*[35] Copyright 2024, American Chemical Society. Abbreviations: Ab: Antibody; DMSN: Dendritic mesoporous silica; EDC: 1-ethyl-3-(3-dimethylaminopropyl) carbodiimide hydrochloride; ECL: Electrochemiluminescence; LFIA: Lateral flow immunoassay; NC: nitrocellulose; NPs: Nanoparticles; oxTMB: Oxidizing 3,3′,5,5′-tetramethyl-benzidine; PB: Prussian blue; PSA: Temperature increase; POD: Peroxidase; TMB: 3,3′,5,5′-tetramethylbenzidine; ΔT: Temperature increase.

overcome the shortcomings of the time-consuming and complicated operation of traditional ELISA detection, Ghosh *et al.*[39] fabricated vanadium disulfide nanosheets linked with biofunctionalised anti-MMP-2 monoclonal antibodies as a label-free electrochemical biosensor for the detection of the MMP-2 protein. The electrochemical impedance spectrometry results confirmed the excellent sensitivity of the sensor as well as its LOD.

Six-transmembrane epithelial antigen of the prostate 1 (STEAP1) is a cell surface protein that functions in cell proliferation or intercellular communication and is usually considered a promising biomarker due to its overexpression in PCa.[40-42] Carvalho *et al.*[43] developed molecularly imprinted polymers on a screen-printed electrode (C-SPE) whose surface was modified with a special nanocomposite and then formed specific template cavities for further STEAP1 detection after an electropolymerisation and enzymatic removal step, resulting in a linear range from 130 pg/mL to 13 μg/mL (**Figure 6**). Overall, the synthesis of the biosensor involves the following four sequential steps: (1) electrochemical activation of C-SPE; (2) immobilisation of the CNT-PAH/PtD complex on the biosensor surface; (3) electropolymerisation of the MIP and NIP materials; and (4) removal of STEAP1.

Glycoproteins such as interleukin-6, which are secreted by diverse kinds of cells, are vital to the PCa process. The overexpression of serum interleukin-6 is linked to the

Table 2. Functionalised nanomaterial-based platforms targeting non-PSA biomarkers for the detection of PCa.

Category	Analytic target	Nanoplatform	Sample	LOD	Linear range	Reference
Cytokine/ protein	MMP-2	2D vanadium disulfide nanosheets	Urine	0.138 fg/mL	10 fg/mL–1 μg/mL	39
	STEAP1	MIP and CNTs PAH/Pt	LNCaP extracts	–	130 pg/mL–13 μg/mL	43
	IL-6	Au/CF electrode	Serum	0.056 fg/mL	1 fg/mL–1 μg/mL	44
	ACP	M-SiO_2@NAC-CuNCs	Serum	0.47 U/L	0.5–28 U/L	45
	PTHrP	Poly(diallyl)dimethylammonium polycations/GSH-AuNPs	Serum	0.3 fg/mL	–	46
Metabolite	Tryptophan and folate metabolites	Surface-carbonized AgNWs	Urine	1.45 nM	–	47
	Sarcosine	$Cu_3(PO_4)_2$:Ce@SOX nanoflowers	Urine	0.226 μM 0.12 μM	0.5–60 μM 0.18–60 μM	54
		Ce-CPNs	Urine	0.14 μM	0.26–33.33 μM	55
		SOx/AuNPs	Serum, urine	0.032 nM	10–40 nM	56
		NA@Ni-LDH NSs	Serum	1.6 pM	5 pM–100 nM, 100 nM–7.9 μM	57
	Citrate	Nano-PIM-1/N-CQDs	Urine	2.2×10^{-8} M	1×10^{-7}–5×10^{-4} M	61
miRNA	miRNA-375, miRNA-148a	CdTe QDs and CDs	Urine	30 aM, 25 aM	0.1–1000 fM	64
	miRNA-183, miRNA-346, miRNA-429, miRNA-484	SOI-NR	Plasma	1.1×10^{-17} M	10^{-18}–10^{-15} M	65
	miR-21, miR-375, miR-141	DNA-AuNPs	Serum	3 pM	0–200 pM	70
	miRNA-143	AuNP/HECA	PC cells, urine	100 aM	1×10^2–1×10^6 aM	71
Exosome	LNCaP.FGC-derived exosome	Ag/IO-GRP	Culture media	134.32 NPs/mL	1×10^2–1×10^6 NPs/mL	73
	PSMA+	Peptide-templated AgNPs	Cell supernatant, serum	37 particles/μL	1×10^2–1×10^8 particles/μL	74
		Au@4-MBA@Ag	Cell supernatant, serum	19 particles/μL	1.2×10^2–2.4×10^3 particles/μL	75
		Fe_3O_4@SiO_2@TiO_2	Cell supernatant, serum	500 particles/μL	0.05–1×10^4 particles/μL	76
	CD81/PSMA/EpCAM+	3D-SiO_2 porous chip	Cell supernatant, serum	2.2×10^2, 1.1×10^3 particles/μL	1×10^5–1×10^9 particles/μL	77

Abbreviations: 2D: Two dimensions; 3D-SiO_2: Three dimensions-silicon dioxide; ACP: Acid phosphatase; Ag/IO-GRP: Ag/iron oxide NP-decorated graphene; AgNWs: Silver nanowire; Au: Gold; Au@4-MBA@Ag: Au@4-mercaptobenzoic acid@Ag; AuNP: Gold nanoparticle; CDs: Carbon dots; CdTe QDs: Cadmium telluride quantum dots; Ce-CPNs: Cerium-based coordination polymer nanoparticles; CF: Carbon fibre; CNT: Carbon nanotube; $Cu_3(PO_4)_2$:Ce@SOX: SOX-inorganic hybrid nanoflowers; DNA-AuNPs: DNA-linked gold nanoprobes; EpCAM: Epithelial cell adhesion molecule; HECA: Hyperbranched rolling circle amplification enhanced CRISPR/Cas12a-based assay; IL-6: Interleukin-6; LNCaP: Lymph node carcinoma of the prostate cells; LNCaP.FGC: The fast colony line, a derivative of LNCaP cell line; MIP: Molecularly imprinted polymers; MMP-2: Matrix metalloproteinase 2; M-SiO_2@NAC-CuNCs: mesoporous silica particles@N-acetyl-l-cysteine capped-copper nanoclusters; NA@Ni-LDH NSs: Nanostructures based on natural asphalt coated with nickel-layered double hydroxide nanosheets; Nano-PIM-1: Nano-polymers of intrinsic microporosity; PAH/Pt: Dendritic platinum nanoparticles; PCa: Prostate cancer; PSA: Prostate-specific antigen; PSMA: Prostate specific membrane antigen; PTHrP: Parathyroid hormone related protein; SOI-NR: Nanoribbon biosensor system based on "silicon-on-insulator" structures; SOx: Sarcosine oxidase; STEAP1: Six-transmembrane epithelial antigen of the prostate 1.

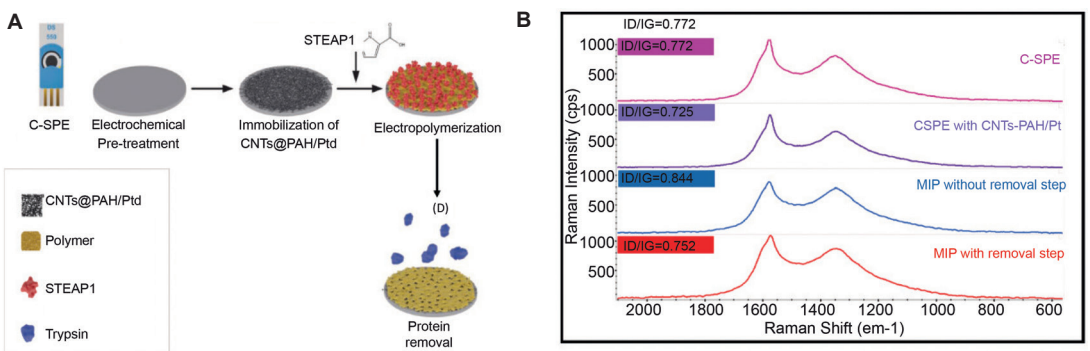

Figure 6. (A) Schematic illustrating the different steps in the construction of an electrochemical biosensor based on a molecularly imprinted polymer for the detection of the STEAP1 protein. (B) Raman spectra for different immobilisation steps. Reprinted with Carvalho *et al.*[43]
Abbreviations: C-SPE: Screen-printed electrode; CNTs: Carbon nanotubes; ID/IG: Intensity ratio of D-band to G-band; MIP: Molecularly imprinted polymer; PAH/Ptd: Dendritic platinum nanoparticles; STEAP1: Six-transmembrane epithelial antigen of the prostate 1.

proliferation and metastatic potential of PCa through androgen receptor activation. Madhu *et al.*[44] presented a flexible electrochemical immunosensor platform integrated with an Au nanoflower structure for detecting interleukin-6. This developed immunosensor could achieve a dynamic detection range of 1 fg/mL to 1 μg/mL with a limit of 0.05 fg/mL and a sensitivity of 62.17 μA/fg/mL after optimisation when verified in clinical PCa patients at stages T3b and T4.

Because acid phosphatase is commonly used as a diagnostic marker of PCa, Chen *et al.*[45] electrostatically assembled N-acetyl-L-Cys-capped copper nanoclusters (NAC-CuNCs) into three-dimensional (3D) mesoporous silica particles (M-SiO2) and finally constructed an enhanced emission platform for "turn off-on" detection of acid phosphatase with a limit of 0.47 U/L. The completed M-SiO2@NAC-CuNCs can be prepared within 2 minutes, so they are highly valuable for practical applications.

Furthermore, early identification of whether PCa is invasive has important guiding significance for clinical treatment and prognosis prediction. With this aim, Dhanapala *et al.*[46] reported an ultrasensitive microfluidic assay for a novel prior biomarker panel including parathyroid hormone-related peptide, which is related to bone metastasis and hypercalcaemia in aggressive PCa. The immunoarray is characterised by the use of a screen-printed carbon sensor electrode, which is covered with 5 nm glutathione-AuNPs and attached to target antibodies. Further studies revealed 83–91% clinical sensitivity and 78–96% specificity for distinguishing between aggressive and indolent PCa and indicated a better predictive effect when the nanoparticles were combined with vascular endothelial growth factor-D.

3.2. Metabolites

Studies have confirmed that specific aromatic metabolites are more present in PCa patients than in healthy individuals. Yu *et al.*[47] presented a novel 3D surface-enhanced Raman spectroscopy (SERS) sensor with a surface-carbonised silver nanowire-stacked filter membrane. Compared with those of normal controls, enhanced SERS intensity derived from semipolar aromatic metabolites including tryptophan metabolites (kynurenine, quinaldic acid, N-acetyltryptophan, N-methyltryptamine and indole-3-acetic acid) and folate metabolites (dihydrofolate and tetrahydrofolate) were observed in PCa urine samples.

Sarcosine (Sar) is commonly considered a biomarker for PCa.[48-50] In the past, many sensors for detecting Sar have emerged, but their practical application was limited by sensitivity, specificity, cost-effectiveness and portability until the advent of nanomaterials and the rapid development of medical combined material cross-research.[51-53] Liu *et al.*[54] introduced organic–inorganic self-assembled nanoflowers (Cu3(PO4)2:Ce@SOX) with inherent fluorescent properties and excellent peroxidase activity. The synthesis of Cu3(PO4)2:Ce@SOX was achieved through a one-step complexation reaction. Initially, enzymes (proteins) form coordination complexes by interacting the amide groups on their backbone with Cu^{2+} and Ce^{3+}. This interaction facilitates the gradual aggregation of protein molecules, which in turn initiates the formation of primary crystals. The proteins function as nucleation inducers for metal phosphate crystals, providing a structural framework for petal-like morphology and effectively serving as an adhesive to bind these structures together. Moreover, they developed a dual-mode multienzyme cascade nanoplatform combining fluorescence and colourimetric methods for the detection of Sar as well as an intelligent smartphone sensor system using cotton swabs for real-time analysis, which was suitable for urine samples (**Figure 7**). Similarly, Wang *et al.*[55] established a tandem dual-mode fluorescence and colourimetric sensor based on Ce(III)-CPNs with regulatable fluorescence and oxidase-like activity for Sar detection. Moreover, Khachornsakkul and Leelasattarathkul[56] presented a photothermal biosensing system integrated with a microfluidic paper-based analytical device to quantitatively detect Sar in urine, plasma, and serum samples. The device uses AuNPs as both a peroxidase-like nanozyme and a photothermal substrate and has a linear range between 10 and 40 nM and an LOD of 32 pM, contributing to its affordability, sensitivity, and user-friendliness. To increase the sensitivity, Farokhi and Roushani[57] synthesised a flower-like core–shell nanostructure based on natural asphalt coated with nickel-layered double hydroxide nanosheets (Ni-LDH NSs) and successfully reduced the calculated LOD of Sar to 1.6 pM.

Citrate is one of the major intermediates in the tricarboxylic acid cycle and is present at lower concentrations in serum and seminal fluid samples from healthy men than in those from PCa patients.[58] It closely participates in the characteristic metabolism of PCa related to the Warburg effect and is widely detected as a complementary biomarker together with PSA.[59] In the work of Afshary *et al.*[60,61] a fast electrochemiluminescence sensor employing a polymer of intrinsic microporosity-1 nanoparticles/nitrogen-doped carbon QDs (nano-PIM-1/N-CQDs) was developed on the basis of the original designed PIM-1 structure to synergistically detect and analyse citrate in urine. The results revealed that the electrochemiluminescence signals were negatively correlated with the concentration of citrate in a certain range from 1.0×10^{-7} M to 5.0×10^{-4} M, with an LOD of 2.2×10^{-8} M.

Linh *et al.*[62] introduced a label-free surface-enhanced Raman scattering sensor based on a 3D plasmonic coral nanoarchitecture with high absorption properties for biofluids followed by direct one-step gold reduction. Through deep learning analysis, the representative SERS spectra of urine from normal men and those from men with PCa were shown to exhibit distinct peak patterns in the regions ranging from 500 to 800 cm^{-1} and 1100 to 1800 cm^{-1} and at 2100 cm^{-1}. This phenomenon is likely caused by the release of different components of metabolites; thus, metabolites can serve as spectral metabolite biomarkers for the detection of PCa. The 3D plasmonic coral nanoarchitecture was further fabricated as a urine test strip, and its integration with a portable handheld Raman system may be a fundamental biofluid detection platform for PCa in the future.

3.3. MicroRNA

Increasing evidence has recently shown that multiple microRNAs (miRNAs) are more sensitive and specific for PCa diagnosis.[63] Differentially expressed miRNAs are essential regulators and indicators of PCa progression biologically.

Jiang *et al.*[64] reported a nanoarchitectonics detection strategy with dumbbell-shaped "C–Ag^{+}–C" and "T–Hg^{2+}–T" hairpin structures targeting miRNA-375 and miRNA-148a in urine, which could be recognised and quantified simultaneously by fluorescent CdTe QDs and carbon dots selectively (**Figure 8**). The system consists of three dumbbell structures (HP1, HP2 and HP3) and two stable hairpin structures (helpers 1 and 2). The dumbbell-shaped hairpin structure that binds C-Ag^{+}-C and T-Hg^{2+}-T is called HP1, which can hybridise with the target miRNA. When the solution contains miRNA-375 and miRNA-148a, these two miRNAs can be recognised by the HP1 ring, Ag^{+} and Hg^{2+} are released, respectively, and then CdTe QDs and carbon dots are detected. The linear range was from 0.1 to 1000 fM, and the LOD reached 30 and 25 aM, respectively,

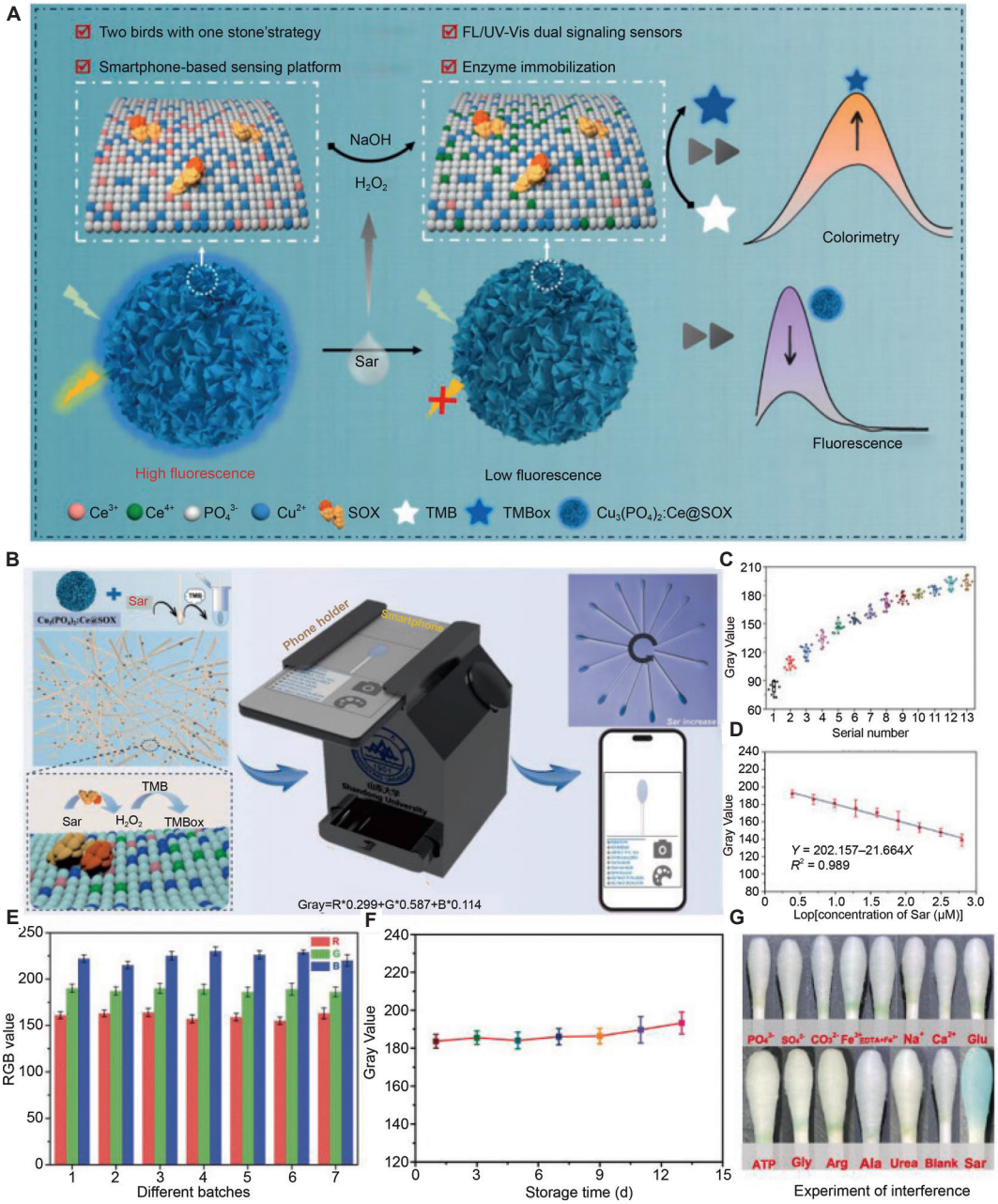

Figure 7. (A) Schematic illustration of the dual-mode fluorescence and colourimetric principle for Sar detection based on self-assembled $Cu_3(PO4)_2$:Ce@SOX. (B) Preparation process of portable cotton swabs (inset: catalytic mechanism) and the smartphone-based visual detection platform. (C, D) Correlation between the grey value and the various concentrations of Sar (the concentrations represented by numbers 1–13 range from 1250 to 2.44 μM). (E) Multiple batches of test swabs prepared for Sar sensors to assess the stability of the RGB value. (f) Stability of the test swabs after storage. (G) Photograph of test swabs with various common ions and small molecules. Reprinted with Liu *et al.*[54] Copyright 2024, Elsevier B.V.

Abbreviations: Ala: Alanine; Arg: Arginase; ATP: Adenosine triphosphate; Ce^{3+}: Cerium(III); Ce^{4+}: Cerium(IV); CO_3^{2-}: Carbonate; $Cu_3(PO4)_2$:Ce@SOX: SOX-inorganic hybrid nanoflowers; Cu^{3+}: Copper(III); Fe^{3+}: Iron(III); FL/UV-VIS: Fluorometer/ultraviolet-visible spectrophotometry; Glu: Glucose; Gly: Glycine; H_2O_2: Hydrogenperoxide; NaOH: Sodium hydroxide; PO_4^{3-}: Phosphate; Sar: Sarcosine; SO_4^{2-}: Sulfate; SOX: Sarcosine oxidase; TMB: 3,3′,5,5′-tetramethylbenzidine; TMBox: Oxidizing 3,3′,5,5′-tetramethyl-benzidine.

with preferable sensitivity (75% and 71%, respectively, versus 50%) and specificity (100% and 94%, respectively, versus 94%) identified in 45 clinical urine samples, demonstrating superior diagnostic value in this cohort compared with serum PSA.

Similarly, Ivanov *et al.*[65] employed silicon-on-insulator structures in a nanoribbon biosensor system for the real-time detection of PCa-associated miRNAs, including miRNA-183, miRNA-346, miRNA-429 and miRNA-484.[66-69] In contrast to antibodies, the DNA oligonucleotide probes used to complement the target miRNAs are more stable and durable chemically, with a detectable concentration of 1.1×10^{-17} M, than conventional ELISA, which can typically detect concentrations of 1×10^{-12} M. Kshirsagar *et al.*[70] also implemented a signal amplification approach combining a

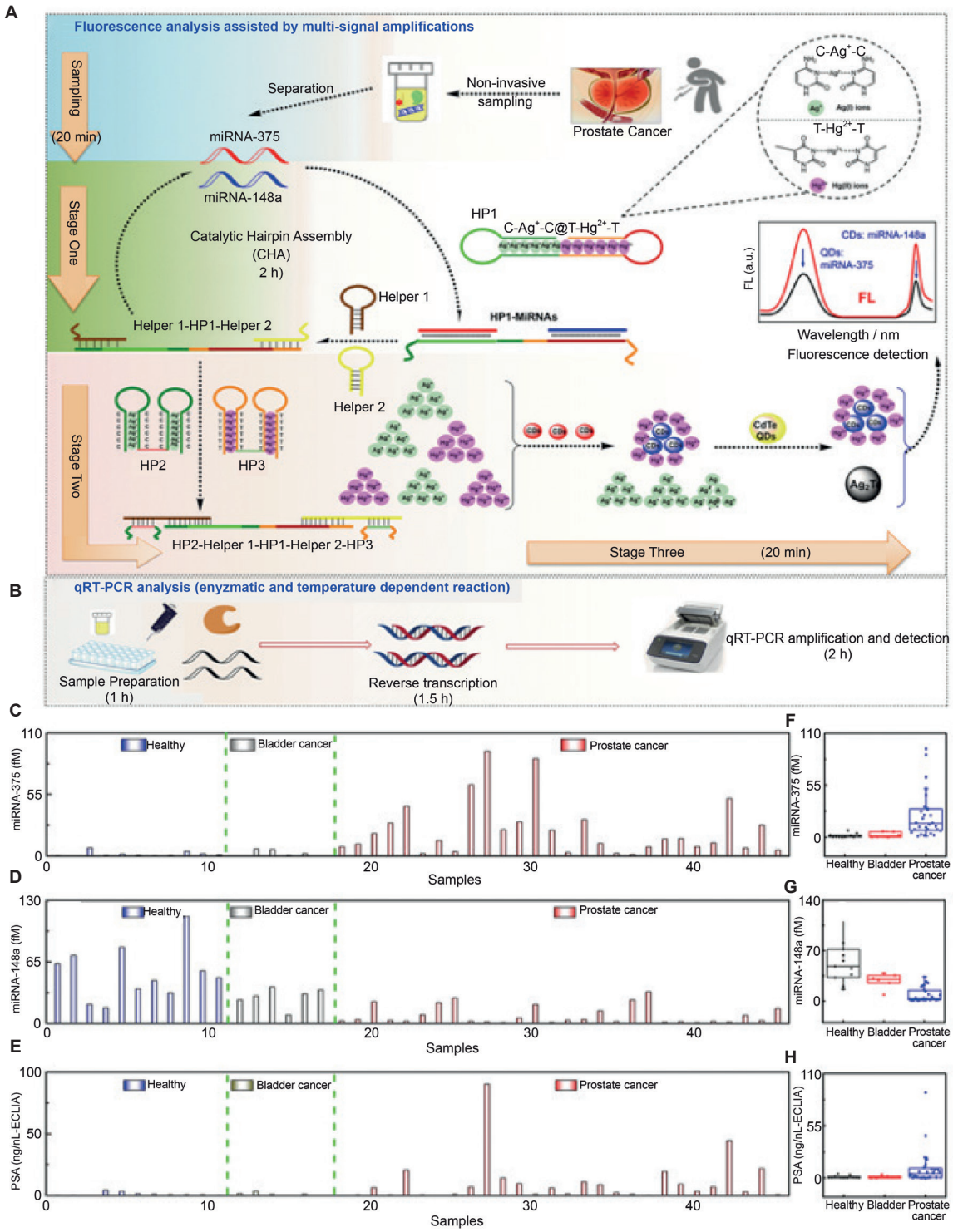

Figure 8. (A, B) Schematic diagram of homogeneous analysis of dual miRNAs assisted by multiple signal amplifications (A) and qRT–PCR analysis (B). (C) Test results for urine miRNA-375 obtained by this method. (D) Results for urine miRNA-148a obtained via this method. (E) Analysis of the serum PSA concentration obtained via a clinical ECL-IA kit. (F–H) Scatter diagrams for urine miRNA-375 (F), urine miRNA-148a (G), and serum PSA (H) in different groups of patients. Reprinted with Jiang *et al.*[64] Copyright 2023, American Chemical Society. Abbreviations: CDs: Carbon dots; ECL: Electrochemical luminescence; ECL-IA: Electrochemiluminescence immunoassay; FL: Fluorometer; HP: Dumbbell structure; QDs: Quantum dots; qRT–PCR: Quantitative real-time polymerase chain reaction.

DNA-linked gold nanoprobe (DNA-AuNPs) and duplex-specific nucleases for the detection of miR-21, miR-375 and miR-141, which are significantly more common in the serum of PCa patients.

Innovatively, Jiang *et al.*[71] combined CRISPR-associated protein 12a (CRISPR/Cas12a)-assisted hyperbranched rolling circle amplification with AuNPs to develop a visual assay for the detection of miRNA-143, which can be observed at

the 1 fM level by the naked eye or with a ultraviolet-visible light (UV–Vis) detector instrument. Moreover, they can also change the padlock probe and crRNA to detect other miRNAs or mRNAs, resulting in outstanding specificity, sensitivity and flexibility.

3.4. Exosomes

Most approaches for the in vitro diagnosis of PCa-targeting exosomes first capture all the exosomes in body fluids and then export the signal. This model inevitably fails to distinguish between normal exosomes and cancer-associated exosomes, thereby confusing the actual detection results.[72] Therefore, its specificity and sensitivity need to be further improved.

Lee *et al.*[73] used silver NP (AgNP)- and magnetic iron oxide NP (IONP)-decorated GRPs as biosensing platforms for detecting PSA^+ exosomes and successfully isolated PCa exosomes from samples.

Prostate specific membrane antigen-positive ($PSMA^+$) exosomes can serve as sensitive biomarkers for PCa detection because of their ability to target PCa cells effectively. To overcome the above drawbacks, Cheng *et al.*[74] constructed an electrochemical biosensor targeting PCa-derived PSMA+ exosomes on the basis of a peptide-templated AgNP nanoprobe. The functionalised peptide probes displayed a wider detection range from 1×10^2 to 1×10^8 particles/μL and a lower detection limit of 37 particles/μL, as verified by clinical samples. Furthermore, Cun *et al.*[75] reported a detection platform comprising PSMA aptamer-modified magnetic beads by combining alkaline phosphatase-induced SERS signal enhancement and hybridised chain reaction amplification. The alkaline phosphatase-induced Ag shell nanostructure acted as an amplifier once the magnetic beads captured the PCa-derived exosomes, and the detection results were obtained within 40 minutes, with a limit of 19 particles/μL (**Figure 9**). To shorten the detection interval, a dual-function platform with off-on signal responses based on Fe3O4@SiO2@TiO2 particles was developed to capture $PSMA^+$ exosomes and quantify them in 20 minutes. Almost half of the detection time was saved, but the sensitivity was lower than that of the above platform, with a detection limit of 5×10^2 particles/μL.[76]

In some cases, exosome detection is constrained by the low binding efficiency and reduced sensitivity of individual markers, such as single-targeting PSMA. Li *et al.*[77] developed a 3D-SiO2 nanoscale porous chip for detecting PCa exosomes that targets multiple tumour-specific markers to remarkably improve the sensitivity for biosensing. Moreover, the adoption of CD81, PSMA, and EpCAM exosomal markers synchronously distinguished benign lesions, early-stage PCa, and advanced PCa and even contributed to tumour staging.

4. Optimising visualisation and imaging technology

Imaging, especially magnetic resonance (MR), is an essential part of PCa diagnostic procedures. To overcome the limitations of traditional imaging strategies for PCa, various types of nanoparticles, ligands and radionuclides free of toxic side effects have been synthesised to selectively target PCa cells.[9]

PSMA is emerging as a prominent imaging biotarget and helps facilitate accurate screening and prognostic prediction of PCa in the imaging field. Wang *et al.*[78] designed a novel noninvasive magnetic resonance/computed tomography/near-infrared fluorescence (MR/CT/NIRF) multimodal contrast agent (AG-Gd@PSMA1 NPs, AGGP) that effectively targets PSMA by superimposing ample Au and Gd motifs into

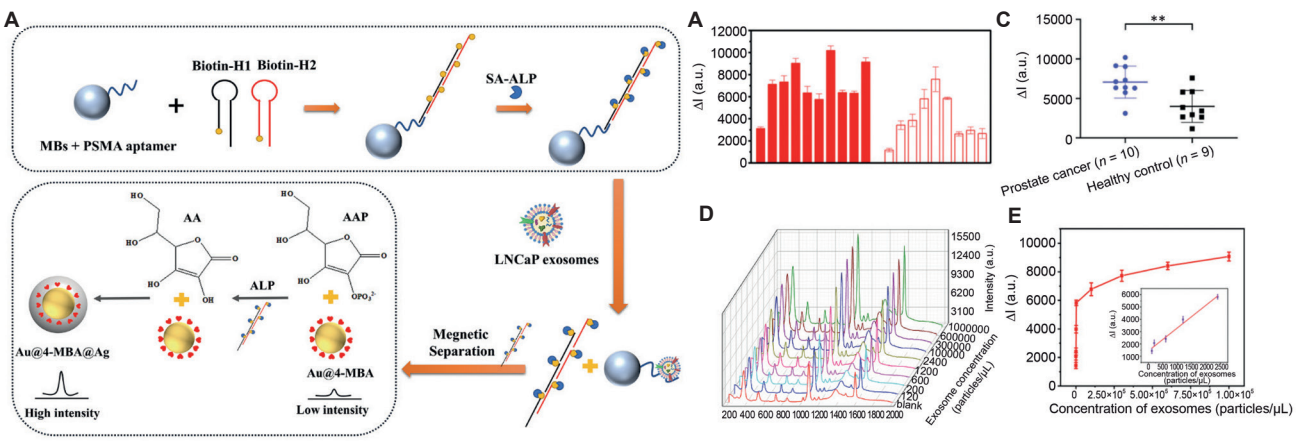

Figure 9. (A) Schematic of the aptamer-induced HCR for the rapid SERS immunoassay of exosomes. Clinical samples detected by the proposed assay. (B) Red bars represent data from prostate cancer patients, white bars represent data from healthy individuals. (C) Purple dots represent the results from prostate cancer patients, and black squares represent the results from healthy controls. (D) SERS spectra of exosomes at different concentrations. Exosome concentrations in curves 1–9: 120, 200, 600, 1200, 2400, 100,000, 300,000, 600,000, and 1,000,000 particles/μL. (E) Linear relationship between the SERS intensity and exosome concentration (120–2400 particles/μL). Reprinted with Cun *et al.*[75] Copyright 2023, American Chemical Society.

Abbreviations: AA: Amino acid; AAP: 2-phospho-L-ascorbic acid trisodium salt; ALP: Alkaline phosphatase; Au@4-MBA: Au@4-mercaptobenzoic acid; Au@4-MBA@Ag: Au@4-mercaptobenzoic acid@Ag; HCR: Hybridized chain reaction; LNCaP: Lymph node carcinoma of the prostate cells; MBA: Mercaptobenzoic acid; MBs: Magnetic beads; PSMA: Prostate-specific membrane antigen; SA-ALP: Streptavidin-labelled alkaline phosphatase; SERS: Surface-enhanced Raman scattering; ΔI: Intensity increase.

a glutathione scaffold, which results in formidable tripe-modal signal augmentation and high security. Liolios *et al.*[79] proposed a proof-of-concept study describing ^{68}Ga-magnetic iron oxide nanoparticles that target PSMA and gastrin-releasing peptide receptor (GRPR) as potential tools for the diagnosis of PCa. The expression of PSMA and GRPR varies among different PCa cell lines. In androgen-independent PC-3 cells, the GRPR gene is highly expressed. Conversely, in androgen-sensitive LNCaP cells, the GRPR gene was negative, and the expression of PSMA was reversed. In this context, the complementary role of the two pharmacophores can address the heterogeneity issue of PCa tumour detection to a certain degree. Cells expressing PSMA or GRPR exhibited specific time-dependent binding, high avidity and high internalisation rates for ^{68}Ga-magnetic iron oxide nanoparticle-NH2. Moreover, toxicity studies of PCa cells revealed low toxicity and minimal haemolysis of red blood cells. Therefore, it is expected to be suitable for PET/MR multimodal imaging.

Iron oxide nanocrystals (IONs) are approved as negative MRI contrast agents; however, their application has been limited because of their low relaxation rate and coherent ferromagnetism. Xie *et al.*[80] reported that Zn-doped IONs possessed optimal T2 MRI contrast performance and significantly enhanced the T2-weighted MRI signal intensity of PCa in a low-toxicity manner. The biosafety of transition-metal-doped IONs was comprehensively assessed through cell viability tests, haemolysis assays, and haematoxylin-eosin (H&E) staining analyses. Ghorbani *et al.*[81] developed potential specific nanomolecular probes by using specific IONPs with PSMA-11 peptides that are clinically used as PCa ligands in imaging. The enhanced contrast in the T2-W images suggests that targeted carboxymethylated dextran (DNP) with PSMA-11-HYNIC peptides (TDNPs) and targeted bovine serum albumin with PSMA-11-HBED peptides (TBNPs) are promising new agents for PSMA$^+$ PCa and the early detection of PCa (**Figure 10**). The most remarkable disparity was observed at 6 hours for PSMA-11-HBED and at 4 hours for PSMA-11-HYNIC. The relative signal enhancement indicated 88.6 ± 3.1% and 80.7 ± 3.2% enhanced contrast between the tumour and muscle regions for TBNPs and TDNPs, respectively, on T2*-W images. The targeted nanoprobes containing PSMA-11 peptides reduced the number of bovine serum albumin and DNP injections by three and two times, respectively. IONPs were coated with bovine serum albumin and carboxymethylated glucan, which significantly reduced their cytotoxicity. Thus, TBNPs offer increased targeting capacity.

Chiral nanomaterials have gained general interest and importance in imaging detection. Li *et al.*[82] fabricated chiral iron oxide supraparticles (Fe3O4 SPs) that acted as high-quality

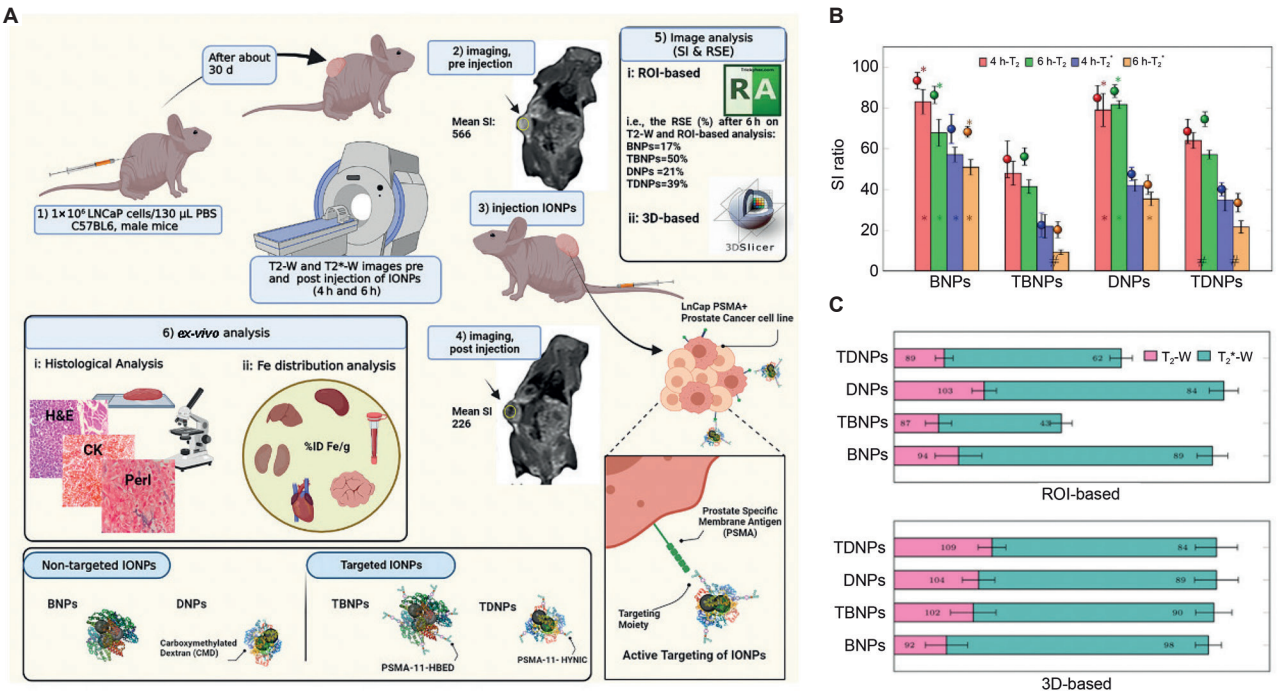

Figure 10. (A) Schematic illustration of the methods used, the chemical structure of targeted and nontargeted IONPs and the active targeting of the targeted IONPs. (B) The mean signal intensity ratio after and before the injection of IONPs presented for the targeted and nontargeted IONPs at both intervals. The bars and the balls indicate the ROI and 3D-driven data, respectively. (C) $SI_{intervals}$ (%): The ratio of signal intensities after 6 hours to those after 4 hours (%). A $SI_{intervals}$ value lower than 100% indicates a greater decrease in the SI after 6 hours than after 4 hours because more iron oxide nanoparticles are taken up. Reprinted with Ghorbani *et al.*[81] Copyright 2023, International Society for Magnetic Resonance in Medicine.

Abbreviations: %ID Fe/g: The injected Fe dose per gram of tissue; 3D: Three dimensions; BNP: Bovine serum albumin; CK: Cytokeratin; DNP: Carboxymethylated-dextran; H&E: Haematoxylin-eosin; IONPs: Iron oxide nanoparticles; LNCaP: Lymph node carcinoma of the prostate cells; PBS: Phosphate buffered saline; Perl: Prussian blue staining; PSMA-11-HBED: A small molecule ligand targeting prostate-specific membrane antigen; PSMA-11-HYNIC: A small molecule ligand targeting prostate-specific membrane antigen; ROI: Regions of interest; RSE: Relative signal enhancement; SI: Signal intensity; TBNP: Targeted BNPs with PSMA-11-HBED peptide; TDNP: Targeted DNPs with PSMA-11-HYNIC peptide.

MRI contrast agents. They reported that D-Fe3O4 SPs presented a twofold lower contrast ratio than L-Fe3O4 SPs did in MR images, which enhanced targeted enrichment in PCa tissues and a 7.7-fold greater affinity for the tumour cell surface receptor CD47. Good biocompatibility is a prerequisite for clinical application. The biosafety of chiral Fe3O4 SPs was evaluated *in vitro* in 4T1 cells and 1640 cells, and the results revealed high stability and low cytotoxicity.

The precise identification of aggressiveness is crucial for determining the prognosis of PCa when it is first diagnosed. Jo *et al.*[83] used methylene blue polyacrylamide nanoparticles to label PCa cells in transgenic adenocarcinoma mouse prostate (TRAMP) models. An in vivo study revealed that methylene blue polyacrylamide nanoparticles can specifically target proliferating cancer cells as contrast agents, allowing photoacoustic imaging to better assess the aggressiveness of PCa. Furthermore, the polyacrylamide nanoparticles utilised in this study are nontoxic, which facilitates their potential clinical application. Martin *et al.*[84] reported that the expression of claudin-3 (CLDN-3) and claudin-4 (CLDN-4) was greater in higher-grade PCa biopsies than in lower-grade PCa biopsies. On the basis of these findings, they designed a dual-loading fluorescent and iron oxide NP-based MRI detection tool with the natural ligand *Clostridium perfringens* enterotoxin (C-CPE) and achieved a 2-fold increase in tumour specificity. This nanoparticle system exhibited minimal toxicity, as evidenced by negligible NP accumulation in the liver and no significant changes in body weight compared with those of untreated mice.

In addition to optimising PCa imaging by applying nanoparticles to enhance lesion-normal tissue contrast or improve cancer cell targeting, a pioneering imaging model for tumour-associated specific flora has recently emerged owing to the definite correlation between the microbiome and PCa.[85, 86] *Escherichia coli* and *Staphylococcus* are the main bacteria that promote prostatitis, and long-term chronic inflammation has been proven to be one of the high-risk factors for PCa.[87-89] Therefore, imaging based on the differential uptake effect of target bacteria on nanoparticles is highly important for the early diagnosis and warning of PCa. Ncapayi *et al.*[90] synthesised ternary AgInSe/ZnS QDs as probes for dual bacterial and cancer bioimaging by near-infrared emission. The QDs were shaped as uniform spheres that accumulated in Staphylococcus aureus and consequently in PCa cells with a diameter of 4.5 ± 0.5 nm and a photoluminescence maximum at 705 nm.

While nano-biomaterials demonstrates promising outcomes, several challenges hinder its clinical translation. Key obstacles include process complexity, cost-effectiveness, and accessibility, which must be addressed to facilitate broader application. Moreover, enhancing the long-term safety and biocompatibility of nanomaterials is crucial, as these factors are fundamental to large-scale clinical implementation, particularly in injectable imaging contrast agents.

5. Conclusions and perspectives

Over the years, clinical methods for PCa screening have mainly focused on PSA detection, digital rectal examination, and imaging, such as ultrasound and MRI. Among them, PSA, as a relatively simple, rapid and noninvasive examination item, is still the most widely used indicator in clinical practice, although it cannot provide highly reliable diagnostic results and cannot be used to accurately determine the degree of malignancy or aggressiveness of PCa.[91] The emergence of nanotechnology has modulated the standard modes of clinical testing, especially in cancer screening and diagnosis. Relying on its unique characteristics, it has successfully improved the effectiveness of various indicators. With the assistance of several well-designed functional nanomaterials, a new paradigm of detection and imaging with ultra-high sensitivity and specificity background has been successfully realised.

At present, nanostructured materials utilised in the detection of PCa are primarily employed to fabricate nanoprobes, nanosensors, and nanosized contrast agents for imaging. The objective is to increase sensitivity, specificity, and stability. While enhancing detection performance, it is essential to prioritise noninvasive operation principles and subsequently consider detection cost, time, operational complexity, and integration capabilities. For example, precious metal nanomaterials such as gold, silver, and platinum are widely used because of their unique properties.[92] Among these materials, AuNPs have been extensively researched for PCa detection.[93] Leveraging their LSPR characteristics allows for the display of varying scattering/absorption features by altering the size, morphology, structure and environmental refractive index of AuNPs, and their colloidal solutions also exhibit diverse colours. Furthermore, the absorption effect of LSPR demonstrates a certain correlation with the quantity of substance added to the test, which manifests as a corresponding change in solution colour enabling visual quantitative detection.

Moreover, the development of composite nanomaterials such as gold-silver bimetals and nanosandwich structures endows them with enhanced catalytic activity, biocompatibility, and stability, making them an exciting avenue for future nanosensor research. In recent years, studies have reported that optimised nanosensors can reduce the detection limit to 0.38 fg/mL or even lower, whereas other methods have successfully shortened the detection time to 5 minutes, resulting in significantly improved efficiency. Additionally, novel nanomaterials, including QDs, UCNPs, magnetic nanomaterials, and carbon/silicon-based nanomaterials, leverage their specific physical properties, such as magnetic, optical, catalytic, and electronic attributes, after integration with PCa-related biomarkers, thereby advancing traditional detection processes.[94]

Notably, targeting diverse markers of PCa represents another trajectory for novel nanodevice development. Owing to recent exploration of new tumour markers coupled with advancements in precision medicine, a wider array of PCa markers has emerged as targets for detection. This serves to enhance specificity within PCa screening from an alternative perspective. For example, tumour-derived exosomes containing specific ribonucleic acids, such as PSA, can be utilised as fresh contents for clinical diagnosis, including miRNA and circulating tumour DNA (ctDNA). Although these innovative markers have are promising for

preclinical trials aimed at specific diagnoses, their extremely low concentration in blood or urine, along with challenges related to their stability following isolation or purification, increases the difficulty of sampling and detection. Importantly, ensuring safety remains a prerequisite prior to large-scale clinical testing. The nanoparticles employed in sensors or probes that serve as hardware components within detection equipment typically do not come into direct contact with the human body; hence, concerns about their biological toxicity are relatively minimal. However, some nanosized imaging contrast agents intended for intravenous injection, especially those comprising metal nanomaterials, necessitate evaluation of their biological toxicity accumulation kinetics and pathophysiological interactions alongside normal cells.

Surprisingly, several markers not mentioned, such as PCA3, are efficient and have been approved in preclinical studies for PCa detection.[95] The discovery of new biomarkers and the development of detection nanotechnologies have facilitated the clinical evaluation of PCa diagnosis. In particular, we pursue the use of fewer samples and noncomplicated processing steps to obtain a higher detection range and a lower detection limit. However, some technical obstacles still hinder the practical application of nanomaterials. A definite expression profile characterising the PCa subtype and stage has still not been fully identified. More perfect detection devices with matched bioassays and uplink systems are needed before the initial application of these biomarkers. In addition, the lack of validation with a large cohort of clinical samples is one of the setbacks in most sensors.

Through this review, we hope to shed light on current nanotechnology-based strategies to design sensors and probes or serve as amplifiers that target PCa biomarkers. We provide new insights for developing more precise nanoformulation-assisted strategies for early PCa detection and diagnosis.

Acknowledgement
None.
Financial support
This work was supported by the Beijing Municipal Administration of Hospitals Incubating Program (No. PX2025071), the Youth Elite Program of Beijing Friendship Hospital (No. YYQCJH2023-1), the Training Fund for Open Projects at Clinical Institutes and Departments of Capital Medical University (No. CCMU2024ZKYXY017), the Talent Development Plan for the Future in Medical-Engineering Integration by the Beijing Research Association for Chronic Diseases Control and Health Education (BRA-CDCHE) and Zhongguancun Talent Association (ZTA) (No. MBRC0012025016), the Science and Technology Special Program of Xicheng District, Beijing (No. XCSTS-T12024-09), the Beijing Key Clinical Specialty Project (No. 20240930), and Young Elite Scientist Sponsorship Program by CAST (No. YESS20240410).
Conflicts of interest statement
The authors declare no competing interests.
Author contributions
Conceptualization: BY, YN, and FZ; *Writing-original draft:* ZZ. *Writing-review & editing:* MC, JL, ZW, and JZ. All authors. All authors read and approved the final manuscript.
Ethics approval and consent to participate
Not applicable.
Consent for publication
Not applicable.
Availability of data
Not applicable.

References

1. Pinsky PF, Parnes H. Screening for prostate cancer. *N Engl J Med.* 2023;388:1405-1414. doi: 10.1056/nejmcp2209151
2. Bergengren O, Pekala KR, Matsoukas K, *et al.* 2022 update on prostate cancer epidemiology and risk factors-a systematic review. *Eur Urol.* 2023;84:191-206. doi: 10.1016/j.eururo.2023.04.021
3. Sandhu S, Moore CM, Chiong E, Beltran H, Bristow RG, Williams SG. Prostate cancer. *Lancet.* 2021;398:1075-1090. doi: 10.1016/S0140-6736(21)00950-8
4. Wei JT, Barocas D, Carlsson S, *et al.* Early detection of prostate cancer: AUA/SUO guideline part I: Prostate cancer screening. *J Urol.* 2023;210:46-53. doi: 10.1097/JU.0000000000003491
5. Schaeffer EM, Srinivas S, Adra N, *et al.* Prostate cancer, version 4.2023, NCCN clinical practice guidelines in oncology. *J Natl Compr Canc Netw.* 2023;21:1067-1096. doi: 10.6004/jnccn.2023.0050
6. Makarov DV, Loeb S, Getzenberg RH, Partin AW. Biomarkers for prostate cancer. *Annu Rev Med.* 2009;60:139-151. doi: 10.1146/annurev.med.60.042307.110714
7. Kuligowska E, Barish MA, Fenlon HM, Blake M. Predictors of prostate carcinoma: Accuracy of gray-scale and color Doppler US and serum markers. *Radiology.* 2001;220:757-764. doi: 10.1148/radiol.2203001179
8. Koo KM, Mainwaring PN, Tomlins SA, Trau M. Merging new-age biomarkers and nanodiagnostics for precision prostate cancer management. *Nat Rev Urol.* 2019;16:302-317. doi: 10.1038/s41585-019-0178-2
9. Lankoff A, Czerwińska M, Kruszewski M. Nanoparticle-based radioconjugates for targeted imaging and therapy of prostate cancer. *Molecules.* 2023;28:4122. doi: 10.3390/molecules28104122
10. Dehghani P, Karthikeyan V, Tajabadi A, *et al.* Rapid near-patient impedimetric sensing platform for prostate cancer diagnosis. *ACS Omega.* 2024;9:14580-14591. doi: 10.1021/acsomega.4c00843
11. Thompson IM, Pauler DK, Goodman PJ, *et al.* Prevalence of prostate cancer among men with a prostate-specific antigen level < or =4.0 ng per milliliter. *N Engl J Med.* 2004;350:2239-2246. doi: 10.1056/nejmoa031918
12. Thompson IM, Ankerst DP, Chi C, *et al.* Assessing prostate cancer risk: Results from the prostate cancer prevention trial. *J Natl Cancer Inst.* 2006;98:529-534. doi: 10.1093/jnci/djj131
13. Funari R, Chu KY, Shen AQ. Multiplexed opto-microfluidic biosensing: Advanced platform for prostate cancer detection. *ACS Sens.* 2024;9:2596-2604. doi: 10.1021/acssensors.4c00312
14. Yeh IH, Shi HF, Darius E, *et al.* Plasmonic biochips with enhanced stability in harsh environments for the sensitive detection of prostate-specific antigen. *J Mater Chem B.* 2024;12:1617-1623. doi: 10.1039/d3tb02303f
15. Gao Y, Wu Y, Huang P, Wu FY. Colorimetric and photothermal immunosensor for sensitive detection of cancer biomarkers based on enzyme-mediated growth of gold nanostars on polydopamine. *Anal Chim Acta.* 2023;1279:341775. doi: 10.1016/j.aca.2023.341775
16. Felici E, Regiart MD, Pereira SV, *et al.* Microfluidic platform integrated with carbon nanofibers-decorated gold nanoporous sensing device for

serum PSA quantification. *Biosensors (Basel).* 2023;13:390.
doi: 10.3390/bios13030390

17. Turan E, Zengin A, Suludere Z, Kalkan N, Tamer U. Construction of a sensitive and selective plasmonic biosensor for prostate specific antigen by combining magnetic molecularly-imprinted polymer and surface-enhanced Raman spectroscopy. *Talanta.* 2022;237:122926.
doi: 10.1016/j.talanta.2021.122926
18. He W, Liu L, Cao Z, *et al.* Shrink polymer based electrochemical sensor for point-of-care detection of prostate-specific antigen. *Biosens Bioelectron.* 2023;228:115193.
doi: 10.1016/j.bios.2023.115193
19. Gao X, Niu T, Xia Q, *et al.* Au-Se bonded nanoprobe for prostate specific antigen detection in serum. *Anal Chim Acta.* 2022;1210:339852.
doi: 10.1016/j.aca.2022.339852
20. Dou Y, Li Z, Su J, Song S. A portable biosensor based on Au nanoflower interface combined with electrochemical immunochromatography for POC detection of prostate-specific antigen. *Biosensors (Basel).* 2022;12:259.
doi: 10.3390/bios12050259
21. Alnaimi A, Al-Hamry A, Makableh Y, Adiraju A, Kanou O. Gold nanoparticles-MWCNT based aptasensor for early diagnosis of prostate cancer. *Biosensors (Basel).* 2022;12:1130.
doi: 10.3390/bios12121130
22. Kekki H, Montoya Perez I, Taimen P, Boström PJ, Gidwani K, Pettersson K. Lectin-nanoparticle concept for free PSA glycovariant providing superior cancer specificity. *Clin Chim Acta.* 2024;559:119689.
doi: 10.1016/j.cca.2024.119689
23. Neves M, Richards SJ, Baker AN, Walker M, Georgiou PG, Gibson MI. Discrimination between protein glycoforms using lectin-functionalised gold nanoparticles as signal enhancers. *Nanoscale Horiz.* 2023;8:377-382.
doi: 10.1039/d2nh00470d
24. Du K, Feng J, Gao X, Zhang H. Nanocomposites based on lanthanide-doped upconversion nanoparticles: Diverse designs and applications. *Light Sci Appl.* 2022;11:222.
doi: 10.1038/s41377-022-00871-z
25. Osuchowski M, Osuchowski F, Latos W, Kawczyk-Krupka A. The use of upconversion nanoparticles in prostate cancer photodynamic therapy. *Life (Basel).* 2021;11:360.
doi: 10.3390/life11040360
26. Li S, Wei X, Li S, Zhu C, Wu C. Up-conversion luminescent nanoparticles for molecular imaging, cancer diagnosis and treatment. *Int J Nanomedicine.* 2020;15:9431-9445.
doi: 10.2147/ijn.s266006
27. Makhneva E, Sklenárová D, Brandmeier JC, *et al.* Influence of label and solid support on the performance of heterogeneous immunoassays. *Anal Chem.* 2022;94:16376-16383.
doi: 10.1021/acs.analchem.2c03543
28. Hu X, Liao J, Shan H, *et al.* A novel carboxyl polymer-modified upconversion luminescent nanoprobe for detection of prostate-specific antigen in the clinical gray zonebase by flow immunoassay strip. *Methods.* 2023;215:10-16.
doi: 10.1016/j.ymeth.2023.05.001
29. Chung S, Revia RA, Zhang M. Graphene quantum dots and their applications in bioimaging, biosensing, and therapy. *Adv Mater.* 2021;33:e1904362.
doi: 10.1002/adma.201904362
30. Sun L, Liu H, Ye Y, *et al.* Smart nanoparticles for cancer therapy. *Signal Transduct Target Ther.* 2023;8:418.
doi: 10.1038/s41392-023-01642-x
31. Korram J, Anbalagan AC, Banerjee A, Sawant SN. Bio-conjugated carbon dots for the bimodal detection of prostate cancer biomarkers via sandwich fluorescence and electrochemical immunoassays. *J Mater Chem B.* 2024;12:742-751.
doi: 10.1039/d3tb02090h
32. Zhu T, Tang Q, Zeng Y, *et al.* Sensitive determination of prostate-specific antigen with graphene quantum dot-based fluorescence aptasensor using few-layer V_2CT_x MXene as quencher. *Spectrochim Acta A Mol Biomol Spectrosc.* 2023;293:122474.
doi: 10.1016/j.saa.2023.122474
33. Min X, Huang S, Yuan C. Dual-color quantum dots nanobeads based suspension microarray for simultaneous detection of dual prostate specific antigens. *Anal Chim Acta.* 2022;1204:339704.
doi: 10.1016/j.aca.2022.339704
34. Ma Z, Guo J, Jiang L, Zhao S. Lateral flow immunoassay (LFIA) for dengue diagnosis: Recent progress and prospect. *Talanta.* 2024;267:125268.
doi: 10.1016/j.talanta.2023.125268
35. Gong H, Gai S, Tao Y, *et al.* Colorimetric and photothermal dual-modal switching lateral flow immunoassay based on a forced dispersion prussian blue nanocomposite for the sensitive detection of prostate-specific antigen. *Anal Chem.* 2024;96:8665-8673.
doi: 10.1021/acs.analchem.4c00862
36. Wang K, Xing X, Ding Y, *et al.* A dual-mode immunosensing strategy for prostate specific antigen detection: Integration of resonance Raman scattering and photoluminescence properties of ZnS:Mn^{2+} nanoprobes. *Anal Chim Acta.* 2022;1205:339775.
doi: 10.1016/j.aca.2022.339775
37. Lichtinghagen R, Musholt PB, Lein M, *et al.* Different mRNA and protein expression of matrix metalloproteinases 2 and 9 and tissue inhibitor of metalloproteinases 1 in benign and malignant prostate tissue. *Eur Urol.* 2002;42:398-406.
doi: 10.1016/s0302-2838(02)00324-x
38. Doldi V, Tortoreto M, Colecchia M, *et al.* Repositioning of antiarrhythmics for prostate cancer treatment: A novel strategy to reprogram cancer-associated fibroblasts towards a tumor-suppressive phenotype. *J Exp Clin Cancer Res.* 2024;43:161.
doi: 10.1186/s13046-024-03081-0
39. Ghosh TN, Rotake DR, Singh SG. 2D vanadium disulfide nanosheets assisted ultrasensitive, rapid, and label-free electrochemical quantification of cancer biomarker (MMP-2). *Nanotechnology.* 2023;34:395501.
doi: 10.1088/1361-6528/acdde9
40. Nolan-Stevaux O, Li C, Liang L, *et al.* AMG 509 (Xaluritamig) an anti-STEAP1 XmAb 2+1 T-cell redirecting immune therapy with avidity-dependent activity against prostate cancer. *Cancer Discov.* 2024;14:90-103.
doi: 10.1158/2159-8290.cd-23-0984
41. Bhatia V, Kamat NV, Pariva TE, *et al.* Targeting advanced prostate cancer with STEAP1 chimeric antigen receptor T cell and tumor-localized IL-12 immunotherapy. *Nat Commun.* 2023;14:2041.
doi: 10.1038/s41467-023-37874-2
42. Xu M, Evans L, Bizzaro CL, *et al.* STEAP1-4 (six-transmembrane epithelial antigen of the prostate 1-4) and their clinical implications for prostate cancer. *Cancers (Basel).* 2022;14:4034.
doi: 10.3390/cancers14164034
43. Carvalho M, Gomes RM, Moreira Rocha S, *et al.* Development of a novel electrochemical biosensor based on plastic antibodies for detection of STEAP1 biomarker in cancer. *Bioelectrochemistry.* 2023;152:108461.
doi: 10.1016/j.bioelechem.2023.10846
44. Madhu S, Han JH, Jeong CW, Choi J. Sensitive electrochemical sensing platform based on Au nanoflower-integrated carbon fiber for detecting interleukin-6 in human serum. *Anal Chim Acta.* 2023;1238:340644.]
doi: 10.1016/j.aca.2022.340644
45. Chen S, Li Z, Xue R, Huang Z, Jia Q. Confining copper nanoclusters in three dimensional mesoporous silica particles: Fabrication of an enhanced emission platform for "turn off-on" detection of acid phosphatase activity. *Anal Chim Acta.* 2022;1192:339387.
doi: 10.1016/j.aca.2021.339387
46. Dhanapala L, Joseph S, Jones AL, *et al.* Immunoarray measurements of parathyroid hormone-related peptides combined with other biomarkers to diagnose aggressive prostate cancer. *Anal Chem.* 2022;94:12788-12797.
doi: 10.1021/acs.analchem.2c02648
47. Yu HJ, Jang E, Woo A, *et al.* Cancer screening through surface-enhanced Raman spectroscopy fingerprinting analysis of urinary metabolites using surface-carbonized silver nanowires on a filter membrane. *Anal Chim Acta.* 2024;1292:342233.
doi: 10.1016/j.aca.2024.342233
48. Hou J, Wang J, Han J, *et al.* An intelligent ratiometric fluorescent assay based on MOF nanozyme-mediated tandem catalysis that guided by contrary logic circuit for highly sensitive sarcosine detection and smartphone-based portable sensing application. *Biosens Bioelectron.* 2024;249:116035.
doi: 10.1016/j.bios.2024.116035

49. Deng M, Yang H, Zhang H, *et al.* Portable and rapid dual-biomarker detection using solution-gated graphene field transistors in the accurate diagnosis of prostate cancer. *Adv Healthc Mater.* 2024;13:e2302117. doi: 10.1002/adhm.202302117
50. Sreekumar A, Poisson LM, Rajendiran TM, *et al.* Metabolomic profiles delineate potential role for sarcosine in prostate cancer progression. *Nature.* 2009;457:910-914. doi: 10.1038/nature07762
51. Hora CS, Tavares APM, Carneiro LPT, Ivanou D, Mendes AM, Sales MGF. New autonomous and self-signaling biosensing device for sarcosine detection. *Talanta.* 2023;257:124340. doi: 10.1016/j.talanta.2023.124340
52. Song P, Shen J, Ye D, *et al.* Programming bulk enzyme heterojunctions for biosensor development with tetrahedral DNA framework. *Nat Commun.* 2020;11:838. doi: 10.1038/s41467-020-14664-8
53. Annese VF, Patil SB, Hu C, *et al.* A monolithic single-chip point-of-care platform for metabolomic prostate cancer detection. *Microsyst Nanoeng.* 2021;7:21. doi: 10.1038/s41378-021-00243-4
54. Liu P, Sun Q, Gai Z, Yang F, Yang Y. Dual-mode fluorescence and colorimetric smartphone-based sensing platform with oxidation-induced self-assembled nanoflowers for sarcosine detection. *Anal Chim Acta.* 2024;1306:342586. doi: 10.1016/j.aca.2024.342586
55. Wang L, Zheng S, Chen Y, Li C, Wang F. Construction of fluorescence and colorimetric tandem dual-mode sensor by modulating fluorescence and oxidase-like activity via valence switching of cerium-based coordination polymer nanoparticles for sarcosine detection. *Mikrochim Acta.* 2023;190:157. doi: 10.1007/s00604-023-05750-x
56. Khachornsakkul K, Leelasattarathkul T. Photothermal biosensing integrated with microfluidic paper-based analytical device for sensitive quantification of sarcosine. *Talanta.* 2024;271:125628. doi: 10.1016/j.talanta.2024.125628
57. Farokhi S, Roushani M. Flower-like core-shell nanostructures based on natural asphalt coated with Ni-LDH nanosheets as an electrochemical platform for prostate cancer biomarker sensing. *Mikrochim Acta.* 2023;190:198. doi: 10.1007/s00604-023-05779-y
58. Galey L, Olanrewaju A, Nabi H, Paquette JS, Pouliot F, Audet-Walsh É. Rediscovering citrate as a biomarker for prostate cancer. *Nat Rev Urol.* 2024;21:573-575. doi: 10.1038/s41585-024-00899-3
59. Bader DA, McGuire SE. Tumour metabolism and its unique properties in prostate adenocarcinoma. *Nat Rev Urol.* 2020;17:214-231. doi: 10.1038/s41585-020-0288-x
60. Afshary H, Amiri M, Marken F, McKeown NB, Amiri M. ECL sensor for selective determination of citrate ions as a prostate cancer biomarker using polymer of intrinsic microporosity-1 nanoparticles/nitrogen-doped carbon quantum dots. *Anal Bioanal Chem.* 2023;415:2727-2736. doi: 10.1007/s00216-023-04672-0
61. Marken F, Carta M, McKeown NB. Polymers of intrinsic microporosity in the design of electrochemical multicomponent and multiphase interfaces. *Anal Chem.* 2021;93:1213-1220. doi: 10.1021/acs.analchem.0c04554
62. Linh VTN, Lee MY, Mun J, *et al.* 3D plasmonic coral nanoarchitecture paper for label-free human urine sensing and deep learning-assisted cancer screening. *Biosens Bioelectron.* 2023;224:115076. doi: 10.1016/j.bios.2023.115076
63. Fabris L, Ceder Y, Chinnaiyan AM, *et al.* The potential of microRNAs as prostate cancer biomarkers. *Eur Urol.* 2016;70:312-322. doi: 10.1016/j.eururo.2015.12.054
64. Jiang P, Bai Y, Yan L, *et al.* Nanoarchitectonics-assisted simultaneous fluorescence detection of urinary dual miRNAs for noninvasive diagnosis of prostate cancer. *Anal Chem.* 2023;95:7676-7684. doi: 10.1021/acs.analchem.3c00701
65. Ivanov YD, Malsagova KA, Goldaeva KV, *et al.* Nanoribbon biosensor-based detection of microRNA markers of prostate cancer. *Sensors (Basel).* 2023;23:7527. doi: 10.3390/s23177527
66. Ueno K, Hirata H, Shahryari V, Deng G, *et al.* microRNA-183 is an oncogene targeting Dkk-3 and SMAD4 in prostate cancer. *Br J Cancer.* 2013;108:1659-1667. doi: 10.1038/bjc.2013.125
67. Ouyang Y, Gao P, Zhu B, *et al.* Downregulation of microRNA-429 inhibits cell proliferation by targeting p27Kip1 in human prostate cancer cells. *Mol Med Rep.* 2015;11:1435-1441. doi: 10.3892/mmr.2014.2782
68. Selth LA, Townley S, Gillis JL, *et al.* Discovery of circulating microRNAs associated with human prostate cancer using a mouse model of disease. *Int J Cancer.* 2012;131:652-661. doi: 10.1002/ijc.26405
69. Fredsøe J, Rasmussen AKI, Thomsen AR, *et al.* Diagnostic and prognostic microRNA biomarkers for prostate cancer in cell-free urine. *Eur Urol Focus.* 2018;4:825-833. doi: 10.1016/j.euf.2017.02.018
70. Kshirsagar P, Seshacharyulu P, Muniyan S, *et al.* DNA-gold nanoprobe-based integrated biosensing technology for non-invasive liquid biopsy of serum miRNA: A new frontier in prostate cancer diagnosis. *Nanomedicine.* 2022;43:102566. doi: 10.1016/j.nano.2022.102566
71. Jiang W, Chen Z, Lu J, Ren X, Ma Y. Ultrasensitive visual detection of miRNA-143 using a CRISPR/Cas12a-based platform coupled with hyperbranched rolling circle amplification. *Talanta.* 2023;251:123784 doi: 10.1016/j.talanta.2022.123784
72. Li X, Corbett AL, Taatizadeh E, *et al.* Challenges and opportunities in exosome research-perspectives from biology engineering and cancer therapy. *APL Bioeng.* 2019;3:011503. doi: 10.1063/1.5087122
73. Lee J, Lee JH, Mondal J, *et al.* Magnetofluoro-immunosensing platform based on binary nanoparticle-decorated graphene for detection of cancer cell-derived exosomes. *Int J Mol Sci.* 2022;23:9619. doi: 10.3390/ijms23179619
74. Cheng W, Sun Y, Zhao G, *et al.* A novel peptide-templated AgNPs nanoprobe for theranostics of prostate cancer. *Biosens Bioelectron.* 2023;223:114978. doi: 10.1016/j.bios.2022.114978
75. Cun F, Huang Z, Lin Q, *et al.* Hybridized chain reaction-amplified alkaline phosphatase-induced Ag-shell nanostructure for the sensitive and rapid surface-enhanced raman scattering immunoassay of exosomes. *Anal Chem.* 2023;95:10025-10033. doi: 10.1021/acs.analchem.3c01337
76. Li Q, Wang Y, Ling L, *et al.* Rapid and specific detection nanoplatform of serum exosomes for prostate cancer diagnosis. *Mikrochim Acta.* 2021;188:283. doi: 10.1007/s00604-021-04934-7
77. Li Q, Wang Y, Xue Y, *et al.* Ultrasensitive analysis of exosomes using a 3D self-assembled nanostructured SiO_2 microfluidic chip. *ACS Appl Mater Interfaces.* 2022;14:14693-14702. doi: 10.1021/acsami.1c22569
78. Wang J, Li L, Li Y, *et al.* PSMA1-mediated ultrasmall gold nanoparticles facilitate tumor targeting and MR/CT/NIRF multimodal detection of early-stage prostate cancer. *Nanomedicine.* 2023;47:102617. doi: 10.1016/j.nano.2022.102617
79. Liolios C, Koutsikou TS, Salvanou EA, *et al.* Synthesis and *in vitro* proof-of-concept studies on bispecific iron oxide magnetic nanoparticles targeting PSMA and GRP receptors for PET/MR imaging of prostate cancer. *Int J Pharm.* 2022;624:122008. doi: 10.1016/j.ijpharm.2022.122008
80. Xie W, Gan Y, Zhang Y, *et al.* Transition-metal-doped hydrophilic ultrasmall iron oxide modulates MRI contrast performance for accurate diagnosis of orthotopic prostate cancer. *J Mater Chem B.* 2022;10:9613-9621. doi: 10.1039/d2tb01860h
81. Ghorbani F, Aminzadeh B, Borji N, Soudmand S, Montazerabadi A. Molecular MR imaging of prostate cancer by specified iron oxide nanoparticles with PSMA-11 peptides: A preclinical study. *J Magn Reson Imaging.* 2024;59:2204-2214. doi: 10.1002/jmri.28949

82. Li C, Zhao J, Gao X, *et al.* Chiral iron oxide supraparticles enable enantiomer-dependent tumor-targeted magnetic resonance imaging. *Adv Mater.* 2023;35:e2308198. doi: 10.1002/adma.202308198
83. Jo J, Salfi E, Folz J, *et al.* Photoacoustic spectral analysis for evaluating the aggressiveness of prostate cancer labeled by methylene blue polyacrylamide nanoparticles. *Biosensors (Basel).* 2023;13:403. doi: 10.3390/bios13030403
84. Martin DT, Lee JS, Liu Q, *et al.* Targeting prostate cancer with Clostridium perfringens enterotoxin functionalized nanoparticles co-encapsulating imaging cargo enhances magnetic resonance imaging specificity. *Nanomedicine.* 2022;40:102477. doi: 10.1016/j.nano.2021.102477
85. El Tekle G, Garrett WS. Bacteria in cancer initiation promotion and progression. *Nat Rev Cancer.* 2023;23:600-618. doi: 10.1038/s41568-023-00594-2
86. Rizzo A, Santoni M, Mollica V, Fiorentino M, Brandi G, Massari F. Microbiota and prostate cancer. *Semin Cancer Biol.* 2022;86:1058-1065. doi: 10.1016/j.semcancer.2021.09.007
87. Brede CM, Shoskes DA. The etiology and management of acute prostatitis. *Nat Rev Urol.* 2011;8:207-212. doi: 10.1038/nrurol.2011.22
88. Salachan PV, Rasmussen M, Fredsøe J, Ulhøi B, Borre M, Sørensen KD. Microbiota of the prostate tumor environment investigated by whole-transcriptome profiling. *Genome Med.* 2022;14:9. doi: 10.1186/s13073-022-01011-3
89. Porter CM, Shrestha E, Peiffer LB, Sfanos KS. The microbiome in prostate inflammation and prostate cancer. *Prostate Cancer Prostatic Dis.* 2018;21:345-354. doi: 10.1038/s41391-018-0041-1
90. Ncapayi V, Ninan N, Lebepe TC, *et al.* Diagnosis of prostate cancer and prostatitis using near infra-red fluorescent AgInSe/ZnS quantum dots. *Int J Mol Sci.* 2021;22:12514. doi: 10.3390/ijms222212514
91. Wang G, Mao X, Wang W, Wang X, Li S, Wang Z. Bioprinted research models of urological malignancy. *Exploration (Beijing).* 2024;4:20230126. doi: 10.1002/exp.20230126
92. Yang X, Li Y, Liu X, He W, Huang Q, Feng Q. Nanoparticles and their effects on differentiation of mesenchymal stem cells. *Biomater Transl.* 2020;1:58-68. doi: 10.3877/cma.j.issn.2096-112X.2020.01.006
93. Awiaz G, Lin J, Wu A. Recent advances of Au@Ag core-shell SERS-based biosensors. *Exploration (Beijing).* 2023;3:20220072. doi: 10.1002/exp.20220072
94. Hu Y, Lv S, Wan J, *et al.* Recent advances in nanomaterials for prostate cancer detection and diagnosis. *J Mater Chem B.* 2022;10:4907-4934. doi: 10.1039/d2tb00448h
95. Kim WH, Lee JU, Jeon MJ, Park KH, Sim SJ. Three-dimensional hierarchical plasmonic nano-architecture based label-free surface-enhanced Raman spectroscopy detection of urinary exosomal miRNA for clinical diagnosis of prostate cancer. *Biosens Bioelectron.* 2022;205:114116. doi: 10.1016/j.bios.2022.114116

Received: October 23, 2024
Revised: December 31, 2024
Accepted: February 25, 2025
Available online: September 22, 2025